Simulation of Ocean Waves and Marine Currents by Smoothed Particle Hydrodynamics Method

Hossein Rashidian

Submitted to the
Institute of Graduate Studies and Research
in partial fulfillment of the requirements for the Degree of

Master of Science
in
Mechanical Engineering

Eastern Mediterranean University
July 2014
Gazimağusa, North Cyprus

Approval of the Institute of Graduate Studies and Research

Prof. Dr. Elvan Yılmaz
Director

I certify that this thesis satisfies the requirements as a thesis for the degree of Master of Science in Mechanical Engineering.

Prof. Dr. Uğur Atikol
Chair, Department of Mechanical Engineering

We certify that we have read this thesis and that in our opinion it is fully adequate in scope and quality as a thesis for the degree of Master of Science in Mechanical Engineering.

Prof. Dr. Hikmet Ş. Aybar
Supervisor

Examining Committee

1. Prof. Dr. Hikmet Ş. Aybar

2. Prof. Dr. Fuat Egelioğlu

3. Assoc. Prof. Dr. Hasan Hacışevki

ABSTRACT

Using the advances in smoothed particle hydrodynamics method in the numerical simulation of the ocean waves and marine currents is the aim of this study. The ocean wave has been proposed to be one of the most commercially feasible energy sources .The modeling of the ocean waves and currents is crucial to recognize wave and marine energy resources. The smoothed particle hydrodynamics (SPH) method and its solver called SPHysics are suitable to analyze the free surface phenomena, because it can easily match with large and complicated geometric and regions. The main idea of the SPH is developing an accurate numerical solution for governing equations with all types of existing boundary conditions by using a set of particles without any mesh. The SPH describes the physical properties of each particle based on the property of neighboring particles. The last version of the serial SPHysics code, V2.2.1, which is based on the SPH method, is applied for numerical modeling in this study. The wave breaking on the sloping beach is endorsed as a validation test case. In this case, the simulation is carried out for three types of breaking wave which are Spilling, Plunging and Surging. According to approach of Grilli et al., the type of breaking wave is obtained due to the slope and dimensionless wave height factor. The results represent a considerable similarity between the computational models and the simulation of breaking waves by the SPHysics. For modeling ocean wave, the wave maker generates waves on the free surface with different periods and amplitude according to the far field Biesel transfer function. In addition, the water surface elevation and the particle velocity components in the sub layers of the still water level can be plotted by Matlab. The results show that the water surface elevation and particle velocity depend on the height of wave and the wave period. It

is important to investigate the marine currents when the waves occur on the free surface of ocean. Finally, the total energy in the waves which consists of potential energy and kinetic energy is analyzed for different ocean waves. In short, total energy will increase as the amplitude of wave maker increases and the wave period decreases.

Keywords: smoothed particle hydrodynamics, SPHysics, ocean wave, wave maker

ÖZ

Bu çalışmada, düzleştirilmiş parçacık hidrodinamik yöntemindeki gelişmeler kullanılarak, okyanus dalgaları ve deniz akımlarının sayısal benzetimi amaçlanmaktadır. Okyanus dalgaları, ticari açıdan uygulanması en uygun enerji kaynaklarından biri olarak öne sürülmüştür. Dalga ve deniz enerji kaynaklarını tanımak için okyanus dalgaları ve akımlarının modellemesi çok önemlidir. Düzleştirilmiş parçacık hidrodinamik (SPH) yöntemi ve çözüm programı SPHysics, serbest yüzey çözümlenmesi için uygundur çünkü büyük ve karmaşık geometrik bölgeler kolayca modellenebilir. SPH'nin ana fikri, temel denklemler için, sınır koşulları ile herhangi bir ağ oluşturmadan, yalnızca parçacıkların bir kümesi kullanılarak sayısal bir çözüm geliştirmektir. SPH, her bir parçacığın fiziksel özelliklerini komşu parçacıkların özelliğine göre tanımlar. Seri SPHysics kodunun son sürümü V2.2.1, SPH yöntemine dayanmaktadır. Bu çalışmada, sayısal modelleme için bu sürüm kullanılmıştır. Geçerleme testi olarak eğimli sahilde dalga kırılması kullanılmıştır. Bu durumda simülason, dalan, kabaran ve dökülen olarak üç tip dalga kırılması için gerçekleştirilmiştir. Grilli ve arkadaşlarının çalışmasına göre, dalga kırılma türü, eğim ve boyutsuz dalga yükseklik faktörü ile elde edilir. Sayısal model ve SPHysics dalga kırılma benzetimi sonuçları arasında önemli bir benzerlik görülmüştür. Okyanus dalgası modellemesi için, dalga üretici, serbest yüzeyde farklı periyotlarda ve uzak alan Biesel transfer fonksiyonuna göre farklı genliklerde dalgalar oluşturur. Buna ek olarak, alt katmanlarda su yüzeyi yükselmesi ve parçacık hız bileşenleri Matlab ile çizilebilir. Sonuçlar, su yüzeyi yükselmesi ve parçacık hızının dalga yüksekliği ve periyoduna bağımlı olduğunu göstermektedir. Bu dalgalar okyanusun serbest yüzeyinde meydana geldiğinde deniz akımlarını

araştırmak önemlidir. Son olarak, dalgalardaki potansiyel ve kinetik enerjinin toplamı, farklı okyanus dalgalarına göre çözümlenmiştir. Kısaca, toplam enerji dalga üreticisinin genliği arttığında ve dalga periyodu azaldığında artmaktadır.

Anahtar Kelimeler: düzleştirilmiş parçacık hidrodinamiği, SPHysics, okyanus dalgası, dalga üretici

ACKNOWLEDGMENT

I am pleased to express my sincerest gratitude to my supervisor Prof. Dr. Hikmet Ş.Aybar for his advice, scientific hints and his continued support and encouragement. His invaluable advice toward becoming a capable professional in my field of study is one of my greatest assets that will carry throughout my life.

I would like to acknowledge all the professors in the Mechanical engineering department of the Eastern Mediterranean University especially Prof. Dr. Uğur Atikol, Prof. Dr. Fuat Egelioğlu, Assoc. Prof. Dr. Hasan Hacışevki and Prof. Dr. İbrahim Sezai.

It is so apropos to thank all my sincere friends especially Baharam Lavi Sefidgare.

Last and most, in loving memory of my parents. Also I express my deepest affection for my wife, Narges who has always supported me.

TABLE OF CONTENTS

LIST OF TABLES

LIST OF FIGURES

LIST OF SYMBOLS

A	Amplitude of wave maker (m)
C	Wave celerity (m/s)
c	Speed of sound (m/s)
d	Still water level (m)
e	Thermal energy (J)
g	Gravity acceleration (m/s^2)
k	Wave number
L	Wave length (m)
m	Mass (Kg)
h	Smoothed length (m)
H_0	Wave height (m)
q	Non dimensional distance between particle
r	Position vector
s	Slope of inclined plan
S_0	Stroke of wave maker (m)
T	Period of wave maker (s)
t	Time (s)
P	Pressure (KPa)
v	Velocity (m/s)
u	Horizontal particle velocity (m/s)
w	Vertical particle velocity (m/s)
W	Kernel function
Z	Elevation (m)

LIST OF SYMBOLS

Greek

α_D	Normalization parameter of kernel function
β	Slope of the beach
δ	Delta function
ξ_0	Surf similarity parameter
Π	Viscosity term
ρ	Density (kg/m^3)
σ	Angular frequency (1/s)
ϕ	Dissipative term

LIST OF ABBREVIATIONS

ALE	Arbitrary Lagrangian-Eulerian
BC	Boundary Condition
BP	Boundary Particle
CFD	Computational Fluid Dynamics
CFL	Courant Fredrich Levy
CSM	Computational Solid Mechanics
DEM	Diffuse Element Method
EFG	Element Free Galerkin
EMEC	European Marine Energy Center
FDM	Finite Difference Method
FEM	Finite Element Method
FVM	Finite Volume Method
ISPH	Incompressible Smoothed Particle Hydrodynamics
MCED	Marine Current Energy Device
MLPG	Meshless Local Petrov-Galerkin
MWS	Mesh Weak Strong
PIM	Point Interpolation Method
RKPM	Reproduced Kernel Particle Method
SPH	Smoothed Particle Hydrodynamics
SPS	Sub Particle Scale
SWL	Still Water Level
WCSPH	Weakly Compressible Smoothed Particle Hydrodynamics
WEC	Wave Energy Conversion

Chapter 1

INTRODUCTION

1.1 Motivation

Nowadays, with global attention being drawn to climate change and the increasing level of greenhouse gas such as Carbone dioxide, the focus on producing electricity from renewable source is once again a significant area of research. Ocean energy, including wave and tidal current energy, can play a major role in the electricity market, providing reliable and sustainable energy.

Today, the world electricity demand is around 17500 TWh and it can be developed 20000 TWh to 80000 TWh of electricity produced by ocean energy such as wave, tidal, marine current, salinity and ocean thermal [1]. The ocean wave has mostly been proposed as the most commercially feasible energy sources. The solar energy causes wind and waves are created by lowing wind over the surface of ocean. Anyone who studies on the ocean knows that the waves are assumed as harmonic and uniform. Various waves with different height and speed are created by the wind has traveled from one way. The best resource of wave occurs in region where strong wind blown over long distances. Using of wave energy date back to 1799 and the wave power was applied by France in 1910. More researches of wave energy became in the 1940s and this kind of renewable energy presented as it can be commercially source in 1990s [2]. The kinetic and potential energy which contained in natural oscillations of ocean waves is converted by an ocean wave energy system. Different

methods have been presented to convert wave energy into practically electrical energy. Some of the early types of the wave power systems are the Salter Cam and a hinged floating system that both of them developed in UK, the wave-powered developed at Scripp's Institution of Oceanography, a pressure-activated submerged generator developed by Kayser in Germany and a pneumatic wave converter originally developed by Masuda in Japan [3].Wave energy conversion (WEC) is one of the most feasible technologies which European Marine Energy Center (EMEC) has identified eight main types of it [see reference 4]. Theoretically, the efficient extraction of the power of ocean waves is possible. Researchers indicate that more than 90 percent of the power wave can be converted into electricity under certain condition by theoretical researches and experiments. The total efficiency of conversion is almost 35 percent as ancillary extraction processes are considered for the ensemble of all waves annually [5].

Another technique to extract energy from the ocean is marine and tidal current energy. Tidal currents are created by changing gravitational pull of the moon and the sun on the world's oceans constantly. Energy from tides is created by the rise and fall of the sea level (tidal range) and tidal current. The tidal range is the difference between high tide and low tide which produces potential energy. The tidal current is the horizontal water movement that generates kinetic energy. The marine currents are created by the tidal current, the breaking wave, the wind, the salinity and temperature difference, the cabelling and the Coriolis Effect. The tidal and marine currents technologies have same principles of operation due to the concept of using kinetic energy from both of them is same [3]. It is essential to study the characteristic parameters of the marine current flow for the successful application of marine current energy devices (MCEDs). Generally, the large marine currents are occurred

adjacent to headland or between landmasses an exceptionally great energy resource is located where the current velocity is at least 2.5 m/s or more [6]. The wind energy extraction technique and the marine current conversion technology share same principle to generate electricity. Approximately, a wind speed of 18 m/s is same in energy density to a marine current of 2 m/s. Thanks to the movements of the tides are known completely, the tidal currents is as a predictable energy resource which can be applied to generate electricity [7].

At this time, the knowledge of the wave energy convertors and marine current energy devices is not completed. Thus many researches are still on going to improve their performance. On the other hand, the experimental observation may be difficult due to the mixture of various physics effects. Therefore numerical simulation provides a popular and proper way to understand flowing fluid behavior and floating devices. Computational Fluid Dynamics (CFD) is a well-developed science to solve fluid mechanics problems. One of well-known method in the CFD is Smoothed Particle Hydrodynamics (SPH) which applies to simulate free surface phenomena. The SPH method, a mesh free and fully Lagrangian technique, was initially presented by Gingold and Monaghan (1977) and Lucy (1977) to study astrophysics problems. Today, this method uses in numerous objects related to mechanics and fluid dynamics. A free surface SPH open source FORTRAN code named the SPHysics in 2007 which applies to model fluid dynamics problems. The open source code is available to free download at www.sphysics.org [8].

1.2 Study Objectives

The main propose of this study is the simulation of the ocean waves by the SPHysics which is suitable to model the free surface phenomena. In fact, it is provided by a description of the SPHysics based on Smoothed Particle Hydrodynamics (SPH) method and modeling the wave breaking on the sloping beach introduces as a validation test case. In addition, the simulation figures of ocean waves with different frequency and wave height, plots of water surface elevation and particle velocity in the sub layers of the still water level and graphs of total energy for each wave will be done in this project.

1.3 Organization of Thesis

To investigate the smoothed particle hydrodynamics (SPH) method as a mesh free method and its recent advances in free surface phenomena and advantages and disadvantages of using the SPH method will be presented in Chapter 2. In Chapter 3, the structure of the SPH code called SPHysics will be introduced. Chapter 4 reviews ocean surface waves and illustrates the numerical modeling of wave braking by last version of SPHysics and introduces the geometry and desired set up of numerical simulation of ocean waves. Chapter 5 consists of the results of this study and the comparison of water surface elevation, particle velocity and energy between four different simulated waves. Finally, the thesis will finish with conclusion and future study in Chapter 6.

Chapter 2

LITRETURE REVIEW

2.1 Introduction

The goal of this literature review is to investigate the smoothed particle hydrodynamics (SPH) method and its recent advances in free surface phenomena. The survey describes numerical simulation and reviews grid base, mesh free methods and different types of them. Also advantages and disadvantages of using the SPH method is a vital part of this chapter.

2.2 Numerical Simulation

In general, there are three approaches in science to describe the physical phenomena; analytical, experimental and numerical simulation. An analytical methodology is the way of studying to obtain exact solutions. Experimental methods use for observation to test scientific hypotheses. Numerical simulation is a crucial approach for solving complex problems with the help of the computer. To solve a problem by numerical simulation, physical phenomena should be simplified and then mathematical model is created by extraction of important parameters. In fact, mathematical model will be governing equations with proper initial conditions or boundary conditions. One of the ways of solving the governing equations that may be partial differential equation, ordinary differential equations or other possible form of equations is numerical algorithm. In the most techniques that need domain discretization, computational frame should be a set of mesh and accuracy of these techniques depend on the mesh pattern and its size. According to domain decomposition and numerical algorithms,

numerical simulation is created by computer code. For actual engineering problems, it is necessary to verify the code with experimental data or theoretical solutions[9].

2.3 Grid-Based Methods

In fluid dynamics, the Eulerian description and the Lagrangian description are two methods for describing of the motion of a fluid and its properties. The Eulerian approach is a field approach that focuses on a certain domain and when different materials pass through that location, it monitors the changing of properties. The Lagrangian approach identifies a material of the fluid and follows its properties as it moves. In grid or mesh based numerical methods such as finite element method (FEM), finite difference method (FDM) and finite volume method (FVM), the generation of the mesh is a vital and prerequisite for the numerical simulation. The elements in FEM, the grids in FDM and the cells in FVM are created by the meshing. The finite element methods (FEM) are the Lagrangian grid methods that mesh is fixed to the material during simulation. On the other hand, FDM and FVM are the Eulerian mesh methods that grid is fixed in space and with time. For decades, the FEM solves the computational solid mechanics (CSM) problems and the FDM has been used as essential tool solver in computational fluid dynamics (CFD). In some application such as simulating hydrodynamics phenomena where exists large deformations or deformable boundaries and free surfaces, the grid based methods are difficult or unsuitable [9].

2.4 Mesh Free Methods

To develop an accurate numerical solution for governing equations with all types of existing boundary conditions using a set of particles without any mesh is the main idea of the mesh free methods. The procedure of mesh free methods shows in Fig.2.1[10]:

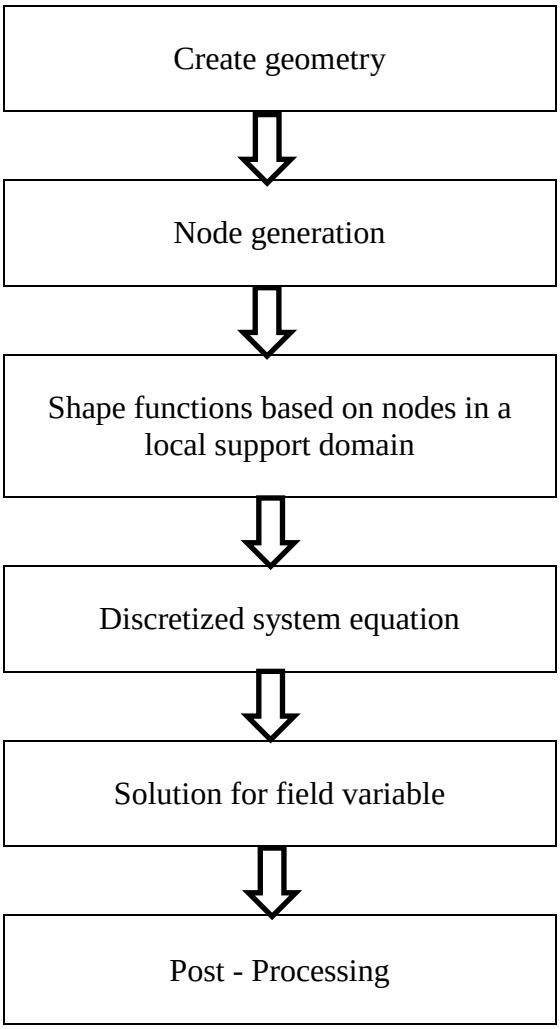

Figure 2.1. Procedure of mesh free methods

The grid free methods have been used for solid mechanics and fluid dynamics by researchers. There are some common features in them, but the methods of approximation and process are different. Some typical mesh free methods have been developed by different researchers such as Smoothed particle hydrodynamics (SPH) method [12-13], diffuse element method (DEM) [14], element free Galerkin (EFG) method [15], reproduced kernel particle method (RKPM) [16], mesh less local Petrov-Galerkin (MLPG) method [17], point interpolation method (PIM) [18], mesh weak strong form (MWS) [19]. The mesh free methods have been classified by Liu and Gu in different ways such as the formulation procedures, the function approximation schemes and the domain representation. Summary of classification of

mash free methods represent in Table 2.1. Future development of the mesh free methods could be in function interpolation or approximation, formulation procedures and combination of them for different types of problem.

Table 2.1. Classification of mesh free methods [10]

Classification	Categories	Example Mesh free methods
Based on formulation procedure	Mesh free methods based on strong-forms of governing equation	Mesh free collocation methods, FPM, etc.
	Mesh free methods based on weak-forms of governing equations	EFG, RPIM, MLPG, LPRIM, etc.
	Mesh free methods based on the combination of weak-form and strong-forms	MWS, etc.
Based on interpolation/approximation method	Mesh free methods using MLS	EFG, MLPG, etc.
	Mesh free methods using integral representation method for function approximations	SPH, etc.
	Mesh free methods using PIM	RPIM, LRPIM, etc.
	Mesh free methods using other mesh free Interpolation schemes	PUFEM, hp-cloud, etc.
Based on domain representation	Domain-type mesh free methods	SPH, EFG, RPIM, MLPG, LRPIM, etc.
	Boundary-type mesh free methods	BNM, LBIE, BPIM, BRPIM, HBRPIM, etc.

2.5 Smoothed Particle Hydrodynamics (SPH) Method

One of the most important methods in mesh free system is smoothed particle method that replaces the fluid with a number of particles to obtain approximate numerical solution of the fluid dynamics equations. In the mathematics, the SPH particles are interpolation points for calculating the properties of the fluid. In the physics, the particles behave like other particles which make material. However the particle method is natural idea, but it is not clear that the interactions between particles can remake the fluid dynamics equations truly. In 1977, Lucy and Gingold and

Monaghan initially developed SPH to simulate astrophysics problems [12-13]. The new SPH algorithm was introduced to apply for a non-dissipative compressible fluid by Gingold and Monaghan [20]. The SPH method can be used for a broad range of fluid dynamics problem such as free surface phenomena due to its Lagrangian nature. The initial attempt to use the SPH for free surface flows was done by Monaghan [21]. Some of the SPH application in free surface phenomena is to study wave propagation [22-26] and breaking wave [27-29]. The stat-of-the-art of SPH for dam break problems was introduced by Gomez-Gesteria et al. [30]. Capone et al. presented a simulation of the wave generated by submarine landslides [31]. There is a current debate about the different approaches base on compressibility of the fluid in free surface problems. Hence, an application of the weakly compressible smoothed particle hydrodynamics (WCSPH) or the fully incompressible smoothed particle hydrodynamics (ISPH) has been compared by different researchers [32-33]. Another open problem in SPH method is about the viscosity [34] which the authors recommend an intermediate approach. As a solution, the viscosity can be depended on vorticity. The SPH methodology can be coupled to other method to create a better result in some problems such as interaction between fluid and structures. For example, Groenenboom et al. introduced a hybrid model to analyze fluid-structure interaction, where SPH model presents the fluid dynamics and the structure is described by Finite Elements Method [35]. In addition, SPH and Arbitrary Lagrangian-Eulerian (SPH-ALE) method is used for analyzing surface flows in a Pelton turbine [36]. Increasing the speed of calculation can be a benefit to use the hybrid models. Thus, the costal wave propagation was studied by Narayanaswamy et al. [25]. They coupled a 2D SPH model and 1D Boussinesq model (FUNWAVE). However the SPH method is mostly applied to solve Navier-Stokes equations.

Thanks to its powerful interpolation, SPH is well studied to describe shallow water equations by De Leffe et al. [26].

2.6 SPHysics Code

A teamwork of researchers at the University of Manchester (UK), the John Hopkins University (USA), the University of Vigo (Spain) and the University of Rome La Sapienza (Italy) presented a free surface SPH open source code called the SPHysics in 2007. This code is written in Fortran 90 and the last update was in January 2011[8]. Moreover, Rising the cost of computational in 3D application can be one of the main disadvantages of SPH methodology which be alleviated by using GRAPHIC Processor Units [37] and parallel computing [38-39]. The parallel version of the SPHysics named ParallelSPHysics released in January 2011 to use for supercomputers and parallel [8]. In addition, the new version of SPHysics called DualSPHysics designed to be executed on GPUs or CPUs. The Programming language of the DualSPHysics is a set of C++, CUDA and JAVA which the last version released in December 2013[40]. As an example of using the DualSPHysics for free surface flow problems, a 3D modeling of wave generated by rockslide was carried by Vacondio et al. [41].

2.7 Pros and Cons

Smoothed particle hydrodynamics method is a simple approach to solve numerical fluid dynamics problems which can provide a wide dynamic range in resolution and density which are unmatched in Eulerian approach. SPH has extremely good conservation properties for energy and linear and angular momentum which is another benefit compared to Eulerian methods. Because of mesh free nature of SPH, it can easily match with large and complicated geometric and regions such as free surface flow problems where are devoid of particles. The density of particles rises in

areas where the material exists. As a result, computational cost and memory storage can be decreased due to focus in these regions during computational effort. Using of SPH in a numerical solver lead to be easy to understand and comparatively simple. For example, negative temperatures or densities may be a problem in grid-based codes, but it does not occur in SPH [42].

The major disadvantage of SPH method is restricted accuracy in multi-dimensional flows due to discrete sums over a small set of nearest neighbors in the approximation of kernel interpolation. SPH is slower solver which is another disadvantage compared to mesh based methods. The time steps and the speed of the sound join together in the weakly compressible fluid dynamics problems. As a result, greater the speed of sound decreases the time steps dramatically. Another generic problem is that the boundary condition implementation is not accurate enough [42].

2.8 Resume

Although there are some disadvantages in numerical simulation with smoothed particle (SPH) method, further to the benefits of mesh less method, it can recommend to researchers for simulating free surface flow phenomena such as ocean wave and marine currents.

Chapter 3

METHODOLOGY

3.1 Introduction

The Smoothed Particle Hydrodynamics (SPH) computes the curve paths of the fluid particles that interact base on the Navier-Stokes equation to predict values of the physical variable of fluid particles. The last version of the SPHysics code, V2.2.1, which is based on the SPH method, is applied for numerical modeling in this study. The aim of this chapter is to describe the SPH method and its solver

3.2 SPH Formulation

In the SPH, the integral of the fluid dynamics equations is solved at each interpolating point which named particles to compute density, velocity, pressure and position of the fluid particles according to the Lagrangian approach. In fact, the physical quantities values of particle are treated as the interpolation of the values of the neighborhood particles. The SPH formulations are obtained by Monaghan [43]. The SPH interpolation of a variable such A(r) is:

$$A(r) = \int_{\varphi} A(r')\mathrm{W}(\mathrm{r} - \mathrm{r}', \mathrm{h})\mathrm{d}r' \qquad \textbf{(3-1)}$$

where W(r-r') is the kernel or weighting function; h is a distance between two neighboring particles named the smoothing length which should be higher than the initial particle separation and it controls the computation domain φ; r is position and dr' is dxdy in two and dxdydz in three dimensions.

In discrete notation, this expression (3-1) leads to an approximation of the function at an interpolation point a.

$$A(r) = \sum_b m_b \frac{A_b}{\rho_b} W(r_a - r_b, h) \quad \textbf{(3-2)}$$

where the summation is over all of the particles b inside the domain of kernel function that fixed by the smoothing length. The m_b and ρ_b are mass and density of particles b respectively. W_{ab} = W (r_a-r_b, h) is the kernel or weight function between two particles a and b when position vector r=r_a.

As one of the benefits for using kernel approximation, the function derivative is calculated analytically:

$$\nabla A(r) = \sum_b m_b \frac{A_b}{\rho_b} \nabla W(r_a - r_b, h) \quad \textbf{(3-3)}$$

3.2.1 The Smoothing Kernel or Weighting Function

The choice of the weight or kernel function plays an essential role in the performance of the SPH. The kernel function must satisfy two conditions [9]:

1) $\int_\varphi W(r - r', h) dr' = 1$
2) $\lim_{h \to 0} W(r - r', h) = \delta(r - r')$

where $\delta(r - r')$ is a delta function.

There are some properties for better efficiency and accuracy of the approximation which kernel function might be required such as:

- Compact support domain: the kernel approximation is transformed from involving integration of the all computation area to a local domain where has much smaller area:

  $W(r - r', h) = 0$ for $\lambda h < r - r'$

where speed of the kernel function is determined by parameter (λ).

- In the compact support domain, the kernel function has non-negative value.
- A monotonically decreasing occurs in kernel function with rising the distance away from its center.
- Symmetric property: the locations where have the equal distance to the center, those will have the equal contributions to the integral.
- Sufficiently smooth: the smoother kernel function and its derivatives have better results and performance when this property uses in approximation.

The kernels are represented as a function of the smoothed length (h) or the non-dimensional distance between particles (q) given by q = $\frac{r_{ab}}{h}$ where r_{ab}= $r_a - r_b$ (the distance between particle a and particle b) and the size of computational domain is controlled by the smoothed length (h). As a result, the accuracy of the SPH interpolation is increased by the polynomials of kernel functions, however, the time of computational also rises.

3.2.2 Equation of Continuity

In the SPH method, changes in the density of fluid are calculated by [43]:

$$\frac{d\boldsymbol{\rho}_a}{dt} = \sum_b m_b v_{ab} \ \nabla_a W_{ab} \quad \textbf{(3-4)}$$

where $v_{ab} = v_a - v_b$ and ∇_a is the gradient for particle a.

3.2.3 Equation of Momentum

In a continuous field, the momentum equation is given by [43]:

$$\frac{dv}{dt} = -\frac{1}{\boldsymbol{\rho}} \ \nabla \mathrm{P} + \mathrm{g} + \ \phi \quad \textbf{(3-5)}$$

where dissipative terms are denoted by ϕ . Also g= (0, 0,-9.81) ms^{-2} refers to the acceleration due to gravity and the pressure gradient in the SPH will be:

$$-\frac{1}{\rho}\ \nabla \mathrm{P} = -\sum_b m_b\left(\frac{P_a}{{\rho^2}_a} + \frac{P_b}{{\rho^2}_b}\right)\nabla_a W_{ab} \quad \textbf{(3-6)}$$

where ρ_b and P_b denote density and pressure of particle b.

3.2.4 Equation of State

The fluid in the SPH method is assumed a weakly compressible by Monaghan [21] and the equation of stae which is the relation between pressure and density is pressented by Monaghan et al. [22]:

$$\mathrm{P} = \mathrm{B}\left[\left(\frac{\rho}{\rho_0}\right)^{\Upsilon} - 1\right] + P_0 \quad \textbf{(3-7)}$$

where P_0 denotes atmospehric pressure which sets usually zero. The coefficent B controls the coperssibility of the fluid and it is given by $B = \frac{{C_0}^2 \rho_0}{\Upsilon}$; Υ=7 for water ; $\rho_0 = 1000$ (kg /m^3) for water. Also c_0 refers to the speed of sound at refrence density (ρ_0) and it is given by c_0=c(ρ_0)= $\sqrt{\frac{\partial P}{\partial \rho}} = \sqrt{\frac{B\Upsilon}{\rho_0}}$ at $\rho = \rho_0$. The selection of B is important due to choose a very small time step based on Courant-Fredrich-Levy (CFL) condition for numerical modeling.

3.2.5 Equation of Moving Particles

Monaghan described moving the particles with a velocity near to the main in their neighborhood by using the XSPH variant [44]:

$$\frac{dr_a}{dt} = v_a + \varepsilon \sum_b m_b \frac{m_b}{\bar{\rho}_{ab}} v_{ba} W_{ab} \quad \textbf{(3-8)}$$

where ε is a free parameter with a range between 0 and 1.

3.2.6 Equation of Themal Energy

The thermal energy of each particle is calculated in SPH using [21]:

$$\frac{de_a}{dt} = \frac{1}{2}\sum_b m_b\left(\frac{P_a}{{\rho^2}_a} + \frac{P_b}{{\rho^2}_b} + \prod_{ab}\right) v_{ab}\nabla_a W_{ab} \quad \textbf{(3-9)}$$

where $\prod_{ab}$ is viscosity term which can be found using the various approaches mentioned before.

3.3 SPHysics

The SPHysics is a solver based on the SPH method that suitable for free-surface problems.

3.3.1 Types of Kernel Function

There are some different kernel functions which use in the SPH method. Four types of famous kernel function which used in the SPHysics are shown in Table 3.1. Also the normalization parameter α_D is different for each kernel function. The kernel function which used in this study is Cubic Spline.

Table 3.1. Four types of kernel function

Type	Formula	$\alpha_D\ (in\ 2D)$
Gaussian	$W(r,h)= \alpha_D \exp(-q^2)$	$\frac{1}{\pi h^2}$
Quadratic	$W(r,h)= \alpha_D [\frac{3}{16}q^2 - \frac{3}{4}q^2 + \frac{3}{4}]$ $0 \le q \le 2$	$\frac{2}{\pi h^2}$
Cubic Spline	$W(r,h)= \alpha_D \begin{cases} 1 - \frac{3}{2}q^2 + \frac{3}{4}q^3 & 0 \le q \le 2 \\ \frac{1}{4}(2-q)^3 & 1 \le q \le 2 \\ 0 & q \ge 2 \end{cases}$	$\frac{10}{7\pi h^2}$
Quintic (Wendland)	$W(r,h)= \alpha_D \left(1 - \frac{q}{2}\right)^4 (2q+1)$ $0 \le q \le 2$	$\frac{7}{4\pi h^2}$

3.3.2 Dissipative Term

According to the dissipative term, the momentum equation can be used for three types of different disspition in SPHysics which are artificial viscosity, laminar viscosity[46] and SPS turbulence[47]. In this study, the artificial viscosity which

was first described by Monaghan [45] is applicable. Because of its simplicity, the artificial viscosity was widely used. The Eq.3-5 can be rewriten as:

$$\frac{dv}{dt} = -\sum_b m_b \left(\frac{P_a}{\rho^2{}_a} + \frac{P_b}{\rho^2{}_b} + \prod_{ab} \right) \nabla_a W_{ab} + g \qquad \textbf{(3-10)}$$

where $\prod_{ab}$ refers to viscosity term which is given by:

$$\prod_{ab} = \begin{cases} \dfrac{-\alpha \bar{c}_{ab} \mu_{ab}}{\bar{\rho}_{ab}} & v_{ab} . r_{ab} < 0 \\ 0 & v_{ab} . r_{ab} > 0 \end{cases} \qquad \textbf{(3-11)}$$

where $\mu_{ab} = \frac{h v_{ab} . r_{ab}}{(r^2{}_{ab} + \zeta^2)}$ and $\zeta^2 = 0.01h^2$. Also $\bar{c}_{ab} = \frac{c_a + c_b}{2}$ refers to the main speed of sound; $\bar{\rho}_{ab} = \frac{\rho_a + \rho_b}{2}$ and α must be adjusted for each problem.

3.3.3 Density Filter

There are large oscillations of pressure in the particles pressure field because of the acoustic waves exist in compressible fluid. Thus two orders of corrections available are Shepard filter [49] and moving least squares [48-49]. The Shepard filter is used in this study due to it has been corrected the density field easily and quickly. In this density filter, its procedure is applied every m time steps (m~30):

$$\rho_a^{new} = \sum_b \rho_b \widetilde{W}_{ab} \frac{m_b}{\rho_b} = \sum_b m_b \widetilde{W}_{ab} \qquad \textbf{(3-12)}$$

where the corrected kernel function uses a zeroth-order:

$$\widetilde{W}_{ab} = \frac{W_{ab}}{\sum_b W_{ab} (\frac{m_b}{\rho_b})} \qquad \textbf{(3-13)}$$

3.3.4 Kernel Renormalization

It is necessary to correct the kernel function periodically when the SPH computes the free surface problems. There are two methods to prevent errors from a kernel function:

3.3.4.1 Kernel Correction

This method was proposed by Liu et al. [52] in an alternative form and then was developed by Bonet and Lok [50] and Vila [51]. Although the linear correction (the first order correction) which modify the kernel function was described by Bonet and Lok [50], a vector variable ($\overrightarrow{f_a}$) that is constant correction and rather than the first order correction, is also recommended by them.

$$\overrightarrow{f_a} = \frac{\sum_b \frac{m_b}{\rho_b} \overrightarrow{f_b} W_{ab}}{\sum_b \frac{m_b}{\rho_b} W_{ab}} \quad \textbf{(3.14)}$$

3.3.4.2 Kernel Gradient Correction

This modified kernel gradient should be applied to determine the forces in the equation of motion in the place of kernel gradient ∇W_{ab} [50-51]:

$$\widetilde{\nabla} W_{ab} = \overrightarrow{L_b} \nabla W_{ab}$$

$$\overrightarrow{L_b} = {M_a}^{-1} \quad \textbf{(3-15)}$$

$$M_a = \sum_b \frac{m_b}{\rho_b} W_{ab} \times (x_a - x_b)$$

3.3.5 Time Stepping

Assume that the continuity (Eq.3-4), momentum (Eq.3-5), position (Eq.3-8) and energy (Eq.3-9) equations in the form:

$$\frac{d\rho_a}{dt} = D_a \quad \textbf{(3-16-a)}$$

$$\frac{dv_a}{dt} = \overrightarrow{F_a} \quad \textbf{(3-16-b)}$$

$$\frac{dr_a}{dt} = \overrightarrow{V_a} \quad \textbf{(3-16-c)}$$

$$\frac{d\rho_a}{dt} = E_a \quad \textbf{(3-16-d)}$$

Four numerical algorithms to apply in SPHysics are predictor-corrector algorithm [44], Verlet algorithm [53], Beeman algorithm [54] and Symplectic algorithm [43].

In this study, the Symplectic algorithm is introduced as time stepping.The first of all, the values of density and acceleration are estimated at the middle time step by:

$$\boldsymbol{\rho}_a{}^{n+\frac{1}{2}} = \boldsymbol{\rho}_a{}^{n} + \frac{\Delta t}{2} \frac{d\boldsymbol{\rho}_a{}^{n}}{dt} \quad \textbf{(3-17-a)}$$

$$\boldsymbol{r}_a{}^{n+\frac{1}{2}} = \boldsymbol{r}_a{}^{n} + \frac{\Delta t}{2} \frac{d\boldsymbol{r}_a{}^{n}}{dt} \quad \textbf{(3-17-b)}$$

where n refers to time step and t = nΔt. Second, the velocity is calculated as:

$$\frac{d(\boldsymbol{\omega}_i\boldsymbol{\rho}_i\boldsymbol{v}_i)^{n+\frac{1}{2}}}{dt} \quad \textbf{(3-18)}$$

The position of particles is estimated at the end of time step by:

$$(\boldsymbol{\omega}_a\boldsymbol{\rho}_a\boldsymbol{v}_a)^{n+1} = (\boldsymbol{\omega}_a\boldsymbol{\rho}_a\boldsymbol{v}_a)^{n+\frac{1}{2}} + \frac{\Delta t}{2} \frac{d(\boldsymbol{\omega}_a\boldsymbol{\rho}_a\boldsymbol{v}_a)^{n+\frac{1}{2}}}{dt} \quad \textbf{(3-19-a)}$$

$$\boldsymbol{r}_a{}^{n+1} = \boldsymbol{r}_a{}^{n+\frac{1}{2}} + \frac{\Delta t}{2} \boldsymbol{v}_a{}^{n+1} \quad \textbf{(3-19-b)}$$

Also, $\frac{d\rho_a^{n+1}}{dt}$ is calculated by the updated values v_a^{n+1} and r_a^{n+1} at the end of the time step.

3.3.6 Variable Time Step

Time step is controlled by the CFL, the viscous diffusion term and the forcing terms [44]. Thus a variable time step is calculated by [22]:

$$\Delta t = 0.3 \min(\Delta t_f, \Delta t_{cv}) \quad \textbf{(3-20)}$$

where Δt_f is based on the force per unit and Δt_{cv} is depend on the CFL and the viscous diffusion term.

3.3.7 Boundary Conditions

In SPHysics, a discrete set of boundary particles establish the boundaries which are three types: Dynamic BCs [55-56], Repulsive BCs [21, 22, and 27] and Periodic Open BCs are still under development.

3.3.7.1 Dynamic Boundary Conditions

In this method [55], boundary particles (BPs) follow the same equations of fluid particles such as momentum equation (Eq.3-5), the continuity equation (Eq.3-4), the equation of state (Eq.3-7) and energy equation (Eq.3-9). Some BPs can be as fixed boundaries or they can move base on some externally imposed function such as wave maker, moving objects …. According to equation (Eq.3-4), the density of the BPs grows up when a fluid particle arrives a boundary. As a result, the pressure also increases due to equation (Eq.3-7). Therefore, the imposed force on the fluid particle raises base on the pressure term of momentum equation (Eq.3-5). Fig.3.1 shows the schematics of dynamics boundary condition.

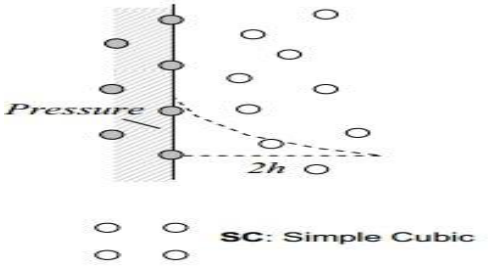

Figure 3.1. Dynamic Boundary Conditions [57]

3.3.7.2 Repulsive Boundary Conditions

This method [21-22, 27] needs to know the position of the neighboring BPs i-1 and i+1 as is shown in Fig.3.2. The force is exerted on the wall by water particle is given by:

$$\vec{f} = \vec{n}\, R(\psi)P(\xi)\varepsilon(z, u) \qquad \textbf{(3-21)}$$

where $\vec{n}$ denotes the normal to the boundary. R(ψ) is the repulsion function:

$$R(\psi) = \frac{1}{h}\ 0.01\ c_i\ \frac{(1-q)}{\sqrt{q}} \quad \text{that} \quad q = \frac{\psi}{2h} \tag{3-22}$$

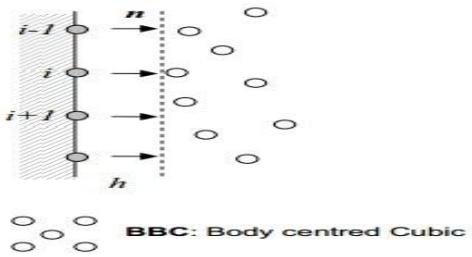

Figure 3.2. Repulsive Boundary Conditions [57]

where ψ is the perpendicular distance between wall and fluid particle and c_i is the sound speed of particle i. When a particle which experiences a constant repulsive force moves parallel to the wall, the function P(ξ) is as follows:

$$P(\xi) = \frac{1}{2}\ (1 + \cos(\frac{2\pi\xi}{\Delta b})) \tag{3-23}$$

Where Δb refers to the distance between two adjacent BPs, ξ denotes an estimate of interpolation location on the line joining (chord) two adjacent BPs. Finally. The value of the force depends on the velocity of normal fluid particle $u_{\perp}$ and the elevation z above SWL (d).

$$\varepsilon\ (z\ ,\ u_{\perp}) = \varepsilon(z\ ) + \varepsilon(u_{\perp}) \tag{3-24}$$

where $\varepsilon(u_{\perp})$ and ε(z) are given by

$$\varepsilon(u_{\perp}) = \begin{cases} 0 & u_{\perp} > 0 \\ |20\ u_{\perp}|\ /\ c_0 & |20\ u_{\perp}| < c_0 \\ 1 & |20\ u_{\perp}| > c_0 \end{cases} \tag{3-25}$$

$$\varepsilon(z) = \begin{cases} 0\ .02 & z \geq 0 \\ |z/h_0| + 0.02 & 0 > z \geq -d \\ 1 & |z/d| > 1 \end{cases} \tag{3-26}$$

Chapter 4

NUMERICAL SIMULATION OF OCEAN WAVES

4.1 Introduction

The ocean surface waves occur in the near to the surface of ocean and they can be classified by height and period. This chapter reviews the ocean surface waves and wind wave and then presents numerical modeling of ocean surface wave by last version of SPHysics.

4.2 Basic Wave Theory

It is important to recognize different between the types of ocean waves. To meet this goal, the characteristics of the wave should be studied. The two dimensional equation of wave is given by [58]:

$$\eta = a\cos(kx - \sigma t)\ ,\ k = 2\pi/\mathrm{L}\ ,\ \ \sigma = 2\pi/\mathrm{T} \qquad \textbf{(4-1)}$$

where η refers to water surface elevations above the SWL (still water level), a denotes wave amplitude which equal half height of wave. Parameter k is wave number and Character σ refers to the angular frequency. L and T are the length wave and wave period respectively (Fig. 4.1). Finally x is the space coordinate and t is time. A summary of linear wave theory is shown in table 4.1.

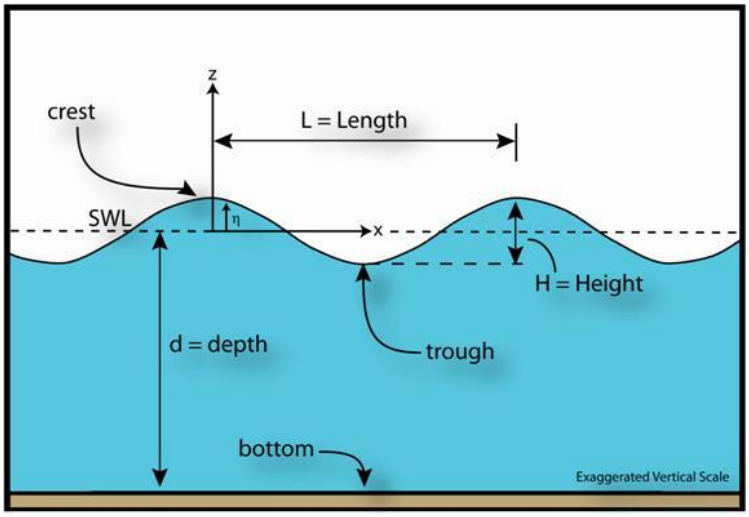

Figure 4.1. The parameters of the wave [60]

Table 4.1. Summary of the linear equations of waves [58]

Relative Depth	Shallow Water $d/L < 1/20$	Transitional Water $1/20 < d/L < 1/2$	Deep Water $d/L > 1/2$
Wave profile	Same as Transitional Water	$\eta = \frac{H}{2}\cos[2kx - \sigma t T] = \frac{H}{2}\cos\theta$	Same as Transitional Water
Wave celerity	$C = \frac{L}{T} = \sqrt{gd}$	$C = \frac{L}{T} = \sqrt{gd} = \frac{gT}{2\pi}\tanh(kd)$	$C = C_0 = \frac{L}{T} = \frac{gT}{2\pi}$
Wave length	$L = T\sqrt{gd} = CT$	$L = \frac{gT^2}{2\pi}\tanh(kd)$	$L = L_0 = \frac{gT^2}{2\pi} = C_0 T$
Horizontal water particle velocity	$u = \frac{H}{2}\sqrt{gd}\cos\theta$	$u = \frac{H}{2}\sigma\frac{\cosh k(z+d)}{\sinh kd}\cos\theta$	$u = \frac{\pi H}{T}e^{kz}\cos\theta$
Vertical water particle velocity	$w = \frac{H\pi}{T}[1+\frac{z}{d}]\sin\theta$	$w = \frac{H}{2}\sigma\frac{\sinh k(z-d)}{\sinh kd}\sin\theta$	$w = \frac{\pi H}{T}e^{kz}\sin\theta$
Horizontal water particle acceleration	$a_x = \frac{H\pi}{T}\sqrt{gd}\sin\theta$	$a_x = \frac{H}{2}\sigma^2\frac{\cosh k(z+d)}{\sinh kd}\sin\theta$	$a_x = 2H\left(\frac{\pi}{T}\right)^2 e^{kz}\sin\theta$
Vertical water particle acceleration	$a_z = -2H\left(\frac{\pi}{T}\right)^2(1+\frac{Z}{d})\cos\theta$	$a_z = \frac{H}{2}\sigma^2\frac{\sinh k(z+d)}{\sinh kd}\cos\theta$	$a_z = -2H\left(\frac{\pi}{T}\right)^2 e^{kz}\cos\theta$
Horizontal water particle displacement	$\xi = -\frac{HT}{4\pi}\sqrt{\frac{g}{d}}\cos\theta$	$\xi = -\frac{H}{2}\frac{\cosh k(z+d)}{\sinh kd}\sin\theta$	$\xi = -\frac{H}{2}e^{kz}\sin\theta$
Vertical water particle displacement	$\xi = \frac{H}{2}[1+\frac{z}{d}]\cos\theta$	$\xi = \frac{H}{2}\frac{\sinh k(z+d)}{\sinh kd}\cos\theta$	$\xi = \frac{H}{2}e^{kz}\cos\theta$
Subsurface pressure	$P = \rho g(\eta - z)$	$P = \rho g\eta\frac{\cosh k(z+d)}{\cosh kd} - \rho gz$	$P = \rho g\eta e^{kz} - \rho gz$

According to wave characteristics, the ocean waves can be classified following Fig. 4.2. The total energy in a wave consists of the potential energy and the kinetic energy. The potential energy is generated by the free surface displacement and the kinetic energy is produced by moving of water particles.

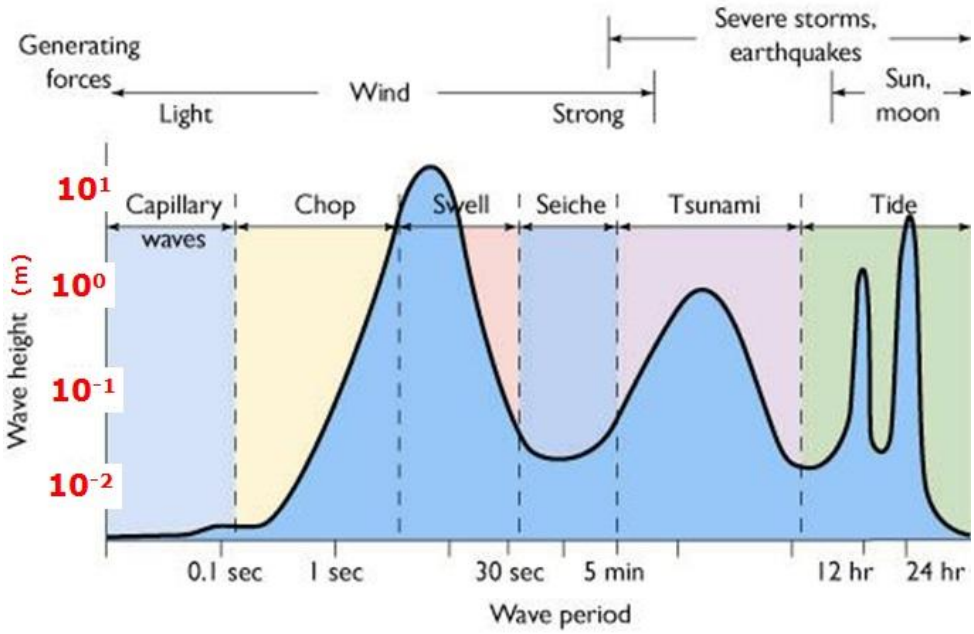

Figure 4.2. Types of wave [61]

4.3 Wave Breaking

The wave breaking phenomena occurs as the amplitude of the wave reaches a maximum level. The wave breaking has large amounts of energy (wind energy) that can be converted to turbulent kinetic energy. Generally, the wave breaking is classified into four types on the sloping beach according to surf similarity parameter (Fig. 4.3 and Table 4.2). The surf similarity parameter is given by [58-59]:

$$\xi_0 = = \frac{\tan\beta}{\sqrt{\frac{H}{L_0}}} \quad \textbf{(4-2)}$$

where $\tan\beta$ denotes the slope of the beach and $\frac{H}{L_0}$ refers to the ratio of the wave height to length of wave for deep water.

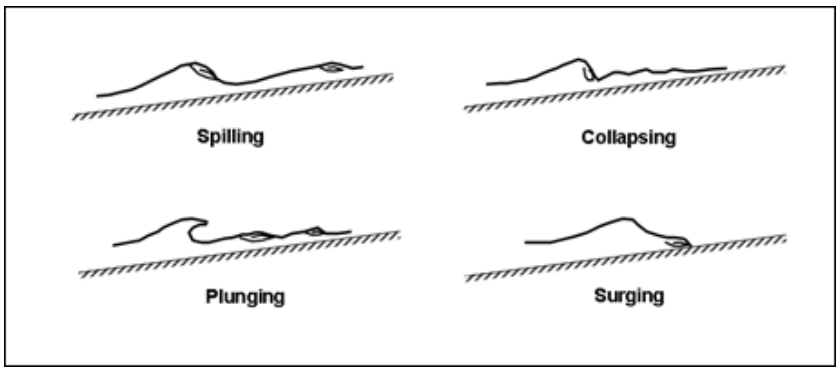

Figure 4.3. Wave breaking types [60]

Table 4.2. Wave breaking types [58]

Breaking Type	Surf Similarity Parameter
Spilling	ξ_o <0.5
Plunging	0.5< ξ_o <2.5
Plunging - Collapsing	2< ξ_o <2.6
Collapsing - Surging	2.5< ξ_o <3.4
Surging	3.4< ξ_o

For solitary waves, a dimensionless slope parameter was presented by Grilli et al. [62] according to a horizontal length scale for length of deep water wave (L_0) :

$$S = 1.521 \frac{S}{\sqrt{H_0'}} \quad \textbf{(4-3)}$$

where s = tan ϕ and $H_0' = \frac{H}{d}$. The breaking wave can be classified by S [62]:

- Spilling breaking: S $<$ 0.025
- Plunging breaking: 0.025 < S $<$ 0.3
- surging breaking: 0.3 < S $<$ 0.37

4.4 Wave Generation

Using of a wave maker is classical method for generating waves in laboratory. There are two types of wave maker to generate the waves: a flap type wave maker and a piston type wave maker [63].

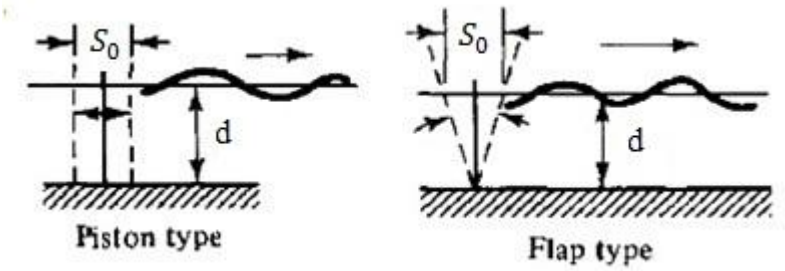

Figure 4.4. Two type of wave maker [63]

Generally, the displacement and velocity of the wave maker is defined by [63]:

$$x_P = x_0 + 0.5\, S_0\, \sin(\sigma t + \theta) \quad \textbf{(4-4)}$$

$$v_P = 0.5\, \sigma\, S_0\, \cos(\sigma t + \theta) \quad \textbf{(4-5)}$$

The function of far field Biesel transfer for the piston type of wave maker is:

$$\frac{H}{S_0} = \frac{2\sinh^2(kd)}{\sinh(kd)\cosh(kd)+kd} \quad \textbf{(4-6)}$$

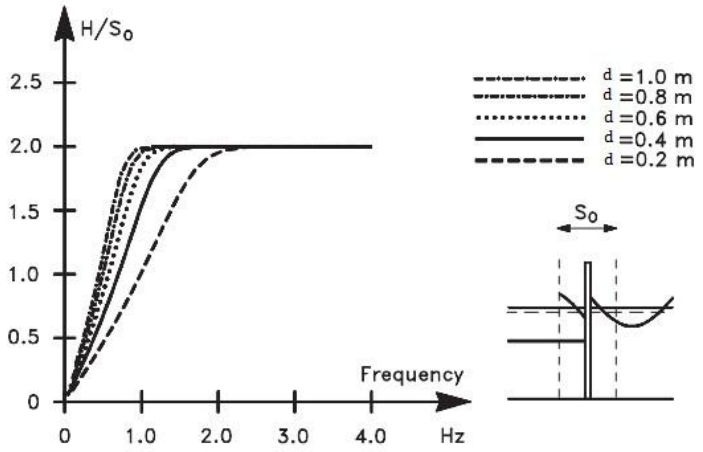

Figure 4.5. Far field Biesel transfer for the piston type of wave maker [63]

4.5 Modeling of Breaking Wave on Sloping Beach

By considering a sloping beach according to Fig. 4.6 and using dimension slope parameter, the breaking waves simulate for their three types and compare with Grilli et al. results [62].

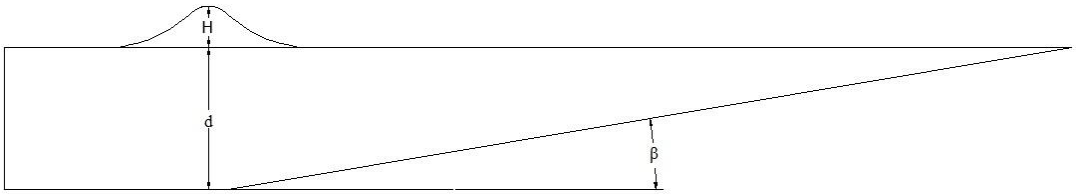

Figure 4.6. Geometry of the simulation of the wave breaking

In this case, the lengths of flat and inclined domains are 1 meter and 6 meter respectively. Also slope of inclined plan (s) is different for each type of breaking wave and will be 1:100, 1: 15 and 1:8.

Table 4.3. Numerical results for three types of breaking wave

s	β	$H_0^{'}$	S	Type of breaking wave
1:100	0.573	0.6	0.0196	Spilling
1:15	3.814	0.6	0.1309	Plunging
1:8	7.125	0.3	0.3471	Surging

Table 4.4. Important parameters of wave maker

d(m) (SWL)	T(s) (Period of wave maker)	A (m) (amplitude of wave maker)	Type of breaking wave
0.2	1.5	0.1	Spilling
0.2	1.5	0.1	Plunging
0.2	1.5	0.05	Surging

According to Eq.4.3, the slope and dimensionless wave height factor are shown in table 4.3. Moreover, the piston type of wave maker is selected and some important parameters are given by table 4.4. The sequence of the spilling, plunging and surging snapshots is presented in Figs. 4.7, 4.9 and 4.11. As shown in Figs. 4.6, 4.7, a decreasing in size of jet occurs when the slope becomes smaller. In fact, the spilling type is formed along the flat shores. Fig. 4.9 represents the simulation of plunging breaker which has a curling top like Fig. 4.8. According to Fig. 4.10, surging breaker takes place along high steep beaches and the wave crest does not curl over. Fig. 4.11 shows the surging simulation which follows the behavior of surging breaker. As a result, there is a considerable similarity between the computational models and the simulation of breaking waves by SPHysics

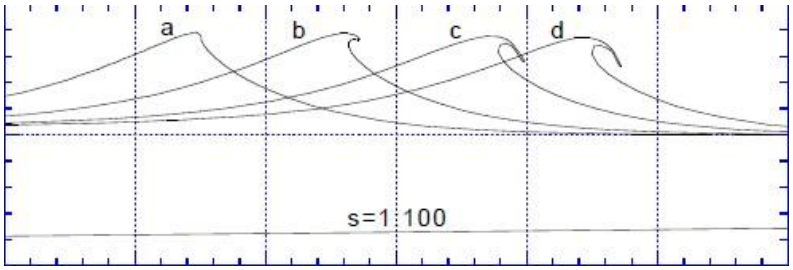

Figure 4.7. Computational model of the spilling type (s=1:100 and $\mathbf{H_0'}$=0.6) [62]

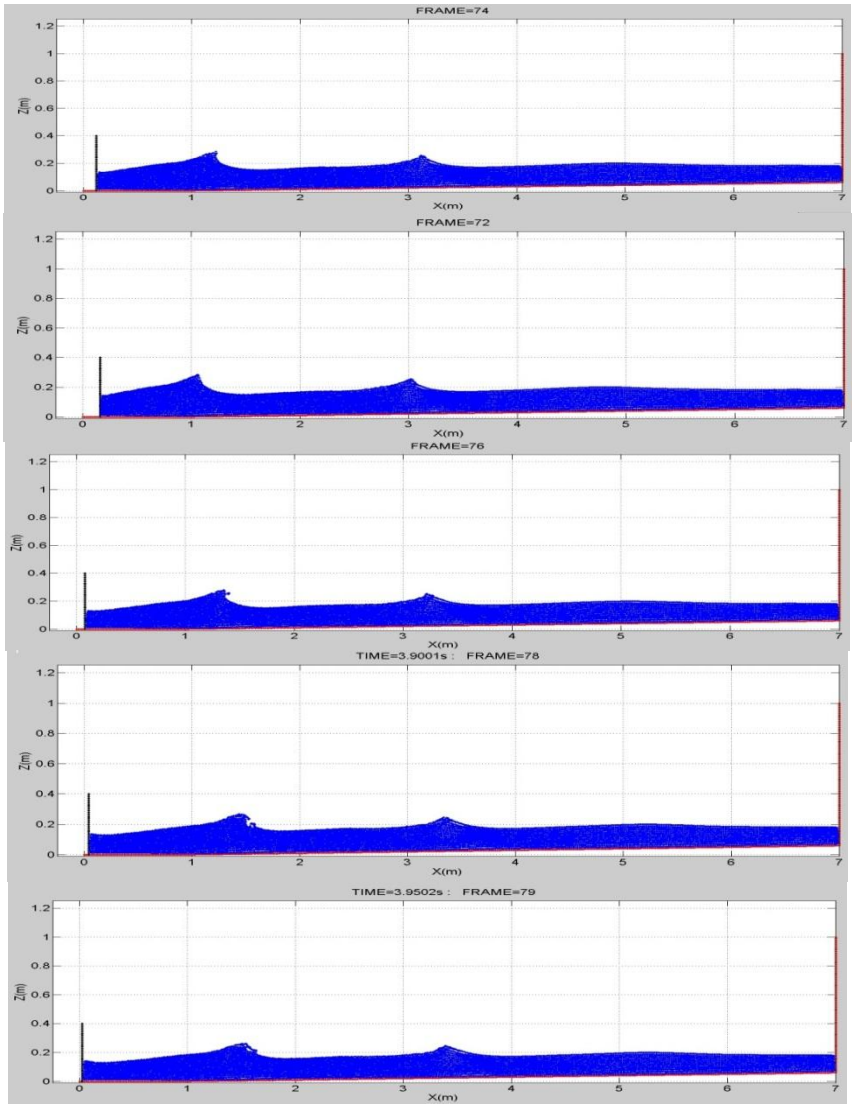

Figure 4.8. Simulation of the spilling type using SPHysics (s=1:100 and $\mathbf{H_0'}$=0.6)

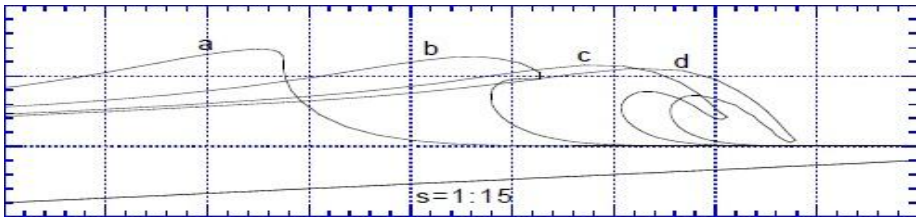

Figure 4.9. Computational model of the plunging type (s=1:15 and $\mathbf{H_0'}$=0.6) [62]

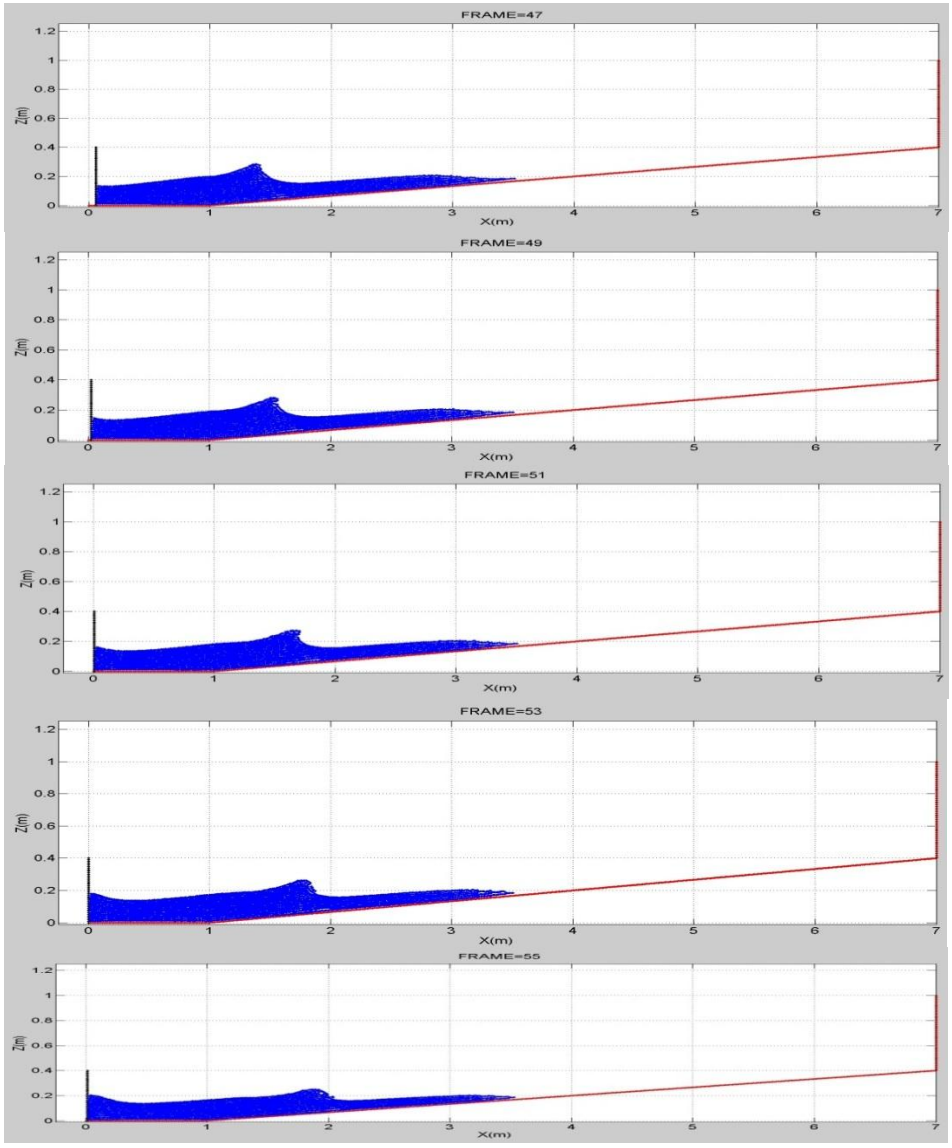

Figure 4.10. Simulation of the plunging type using SPHysics (s=1:15 and $\mathbf{H_0'}$=0.6)

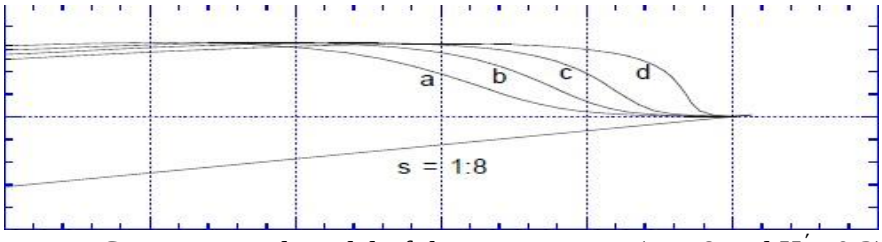

Figure 4.11. Computational model of the surging type (s=1:8 and $\mathbf{H_0'}$=0.3) [65]

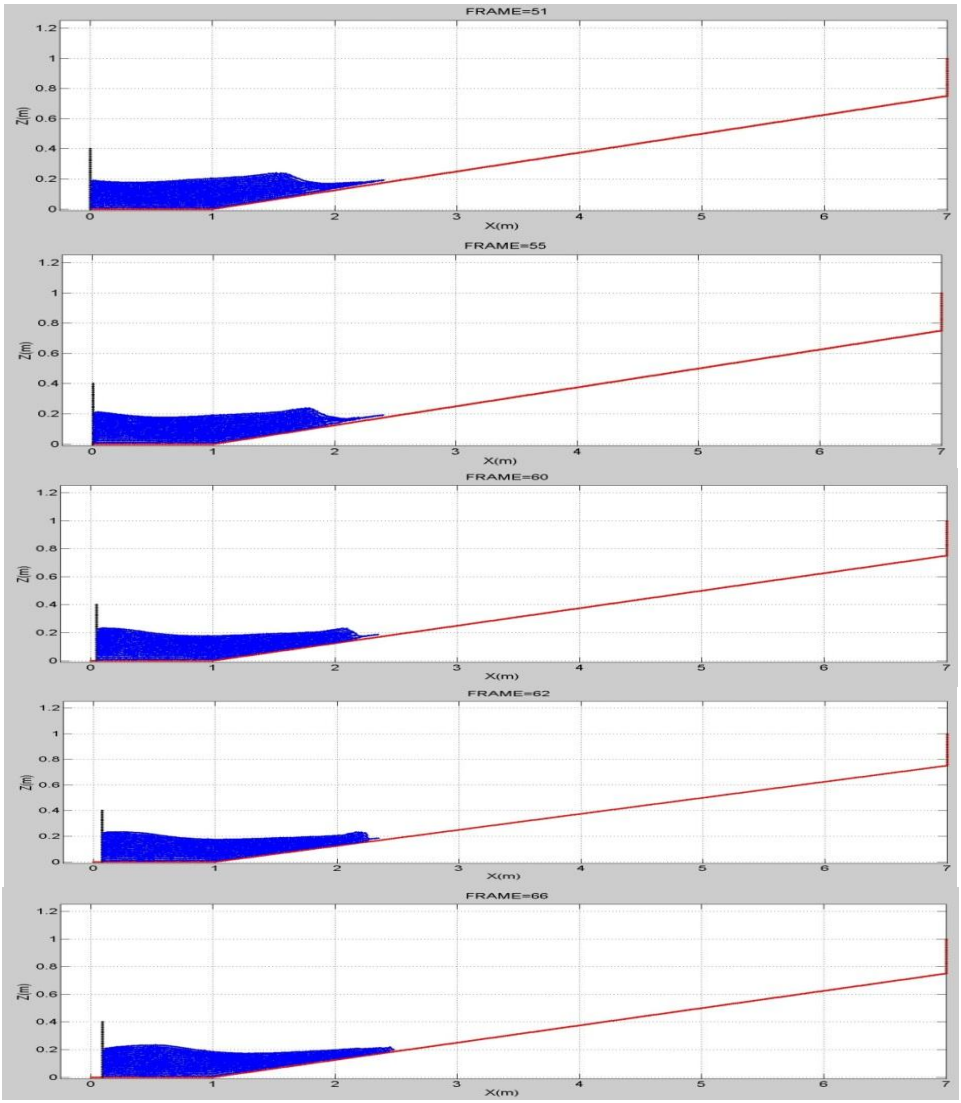

Figure 4.12. Simulation of the surging type using SPHysics (s=1:8 and $\mathbf{H_0'}$=0.3)

4.6 Modeling of Ocean Waves

In this problem, the ocean waves are simulated by Serial SPHysics V2.2.1-2D for different wave frequency and wave height and the elevation of water surface and velocity of particle are evaluated. Moreover, total energy for each ocean wave which consists of potential energy and kinetic energy is analyzed.

4.6.1 Geometry of Simulation

The geometry of a two dimensional numerical simulation is shown in Fig. 4.13. According to this figure, the length of the flume is 20 meter and the water depth is 0.4 meter. A piston type of wave maker which has an initial position of paddle center (x_0), is located on the left and its length of paddle is 0.65 meter.

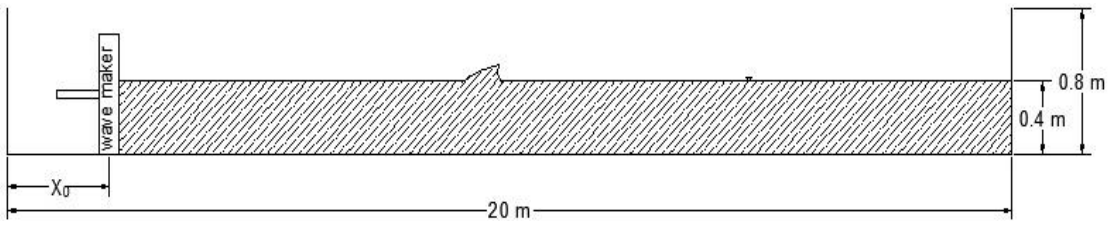

Figure 4.13. Geometry of the simulation of the ocean waves

4.6.2 Numerical Setup and Assumption

During the simulation, some numerical parameters such as speed of sound, CFL number and time of simulation will be constant and follow by table 4.4.In this study, the weakly compressible, the Dynamic BC and the Shepard will be as the equation of state, the boundaries condition and the density filter respectively. Also the cubic-spline kernel function which is the most commonly used kernel is chosen and time stepping algorithm is Symplectic.

Table 4.5. Numerical parameters of the simulation of ocean wave

Coefficient of speed of sound	0.16
CFL Number	0.2
Maximum Time of simulation	10 second

Chapter 5

RESULTS AND DISCUSSION

5.1 Introduction

This chapter is statement of observation, including the simulation figures of ocean waves with different frequency and wave height, plots of water surface elevation and velocity in the sub layers of the still water level and graphs of total energy for each wave. In addition, the comparison between four different simulated waves is presented.

5.2 Simulations of Ocean Surface Waves

In this study, the simulation of ocean waves is carried out for different four cases which make with different periods and amplitudes of wave maker as shown in table 5.1. The behavior of wave propagation for the different cases of simulation is depicted in Figs.5.1-5.4.

Table 5.1. Four cases of simulation of waves

case	Period of wave maker (S)	Amplitude of wave maker (m)
1	1	0.25
2	2	0.25
3	1	0.125
4	2	0.125

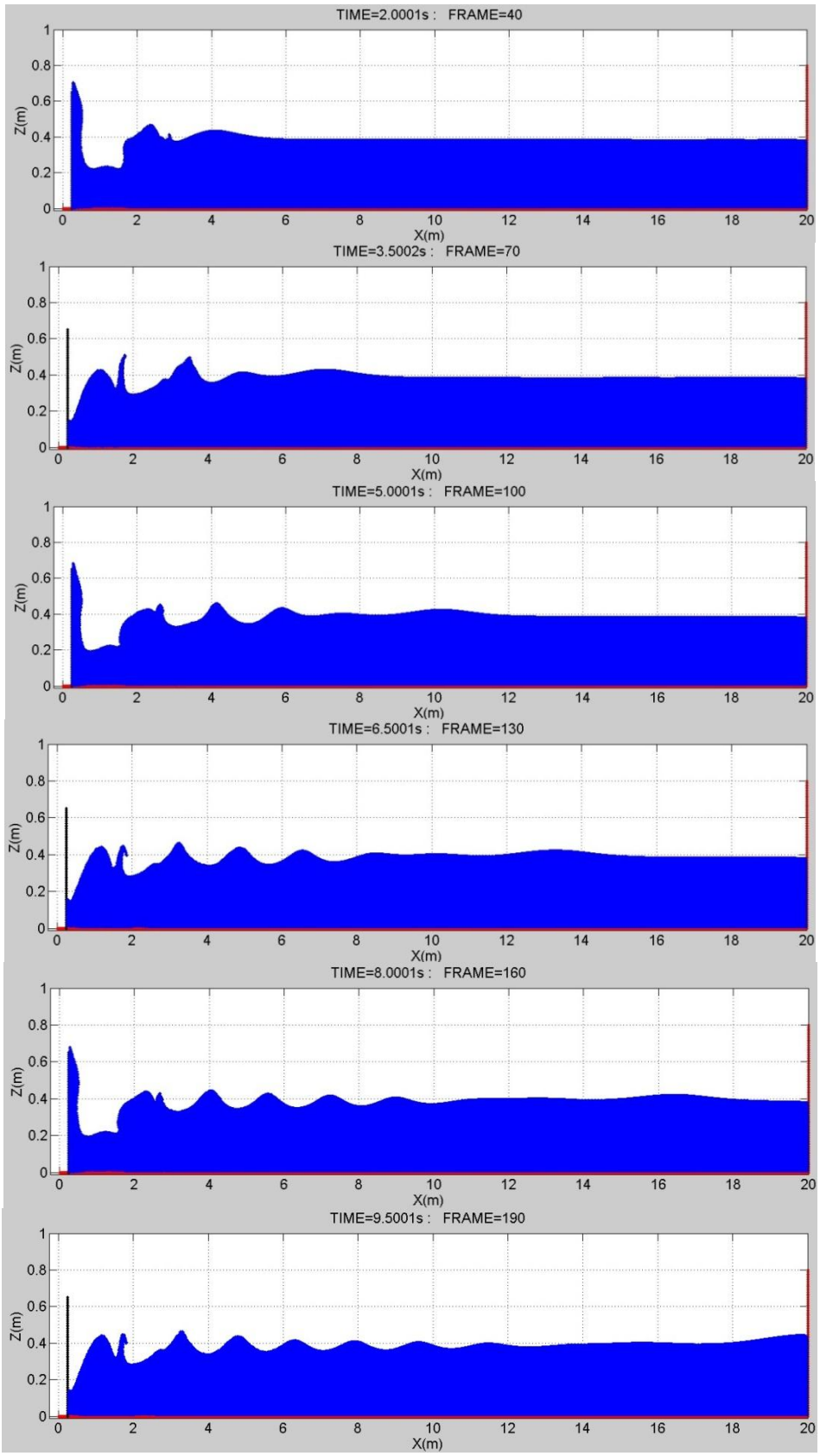

Figure 5.1. Simulation of the wave with T=1s and A=0.25m (case1)

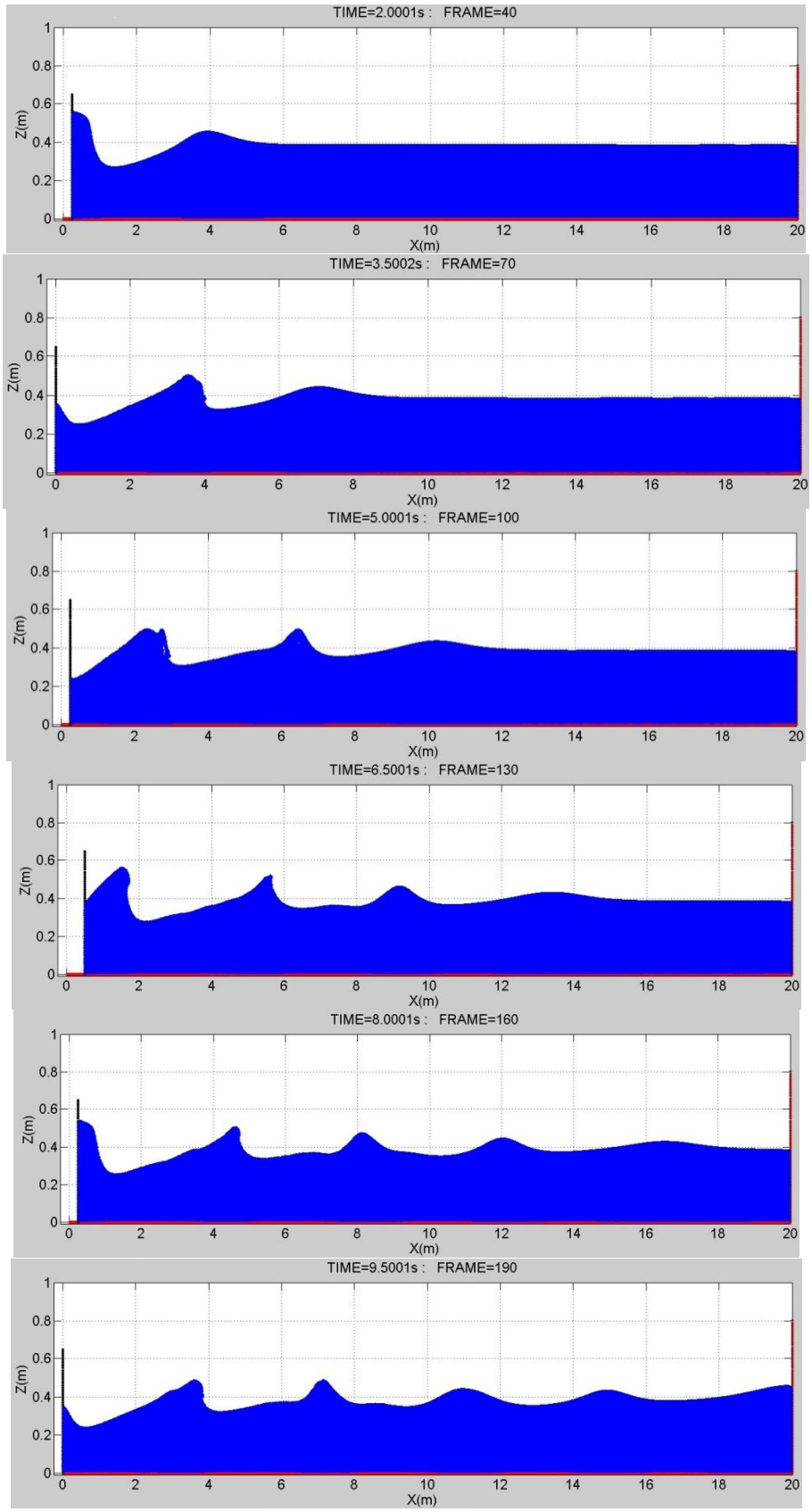

Figure 5.2. Simulation of the wave with T=2s and A=0.25m (case2)

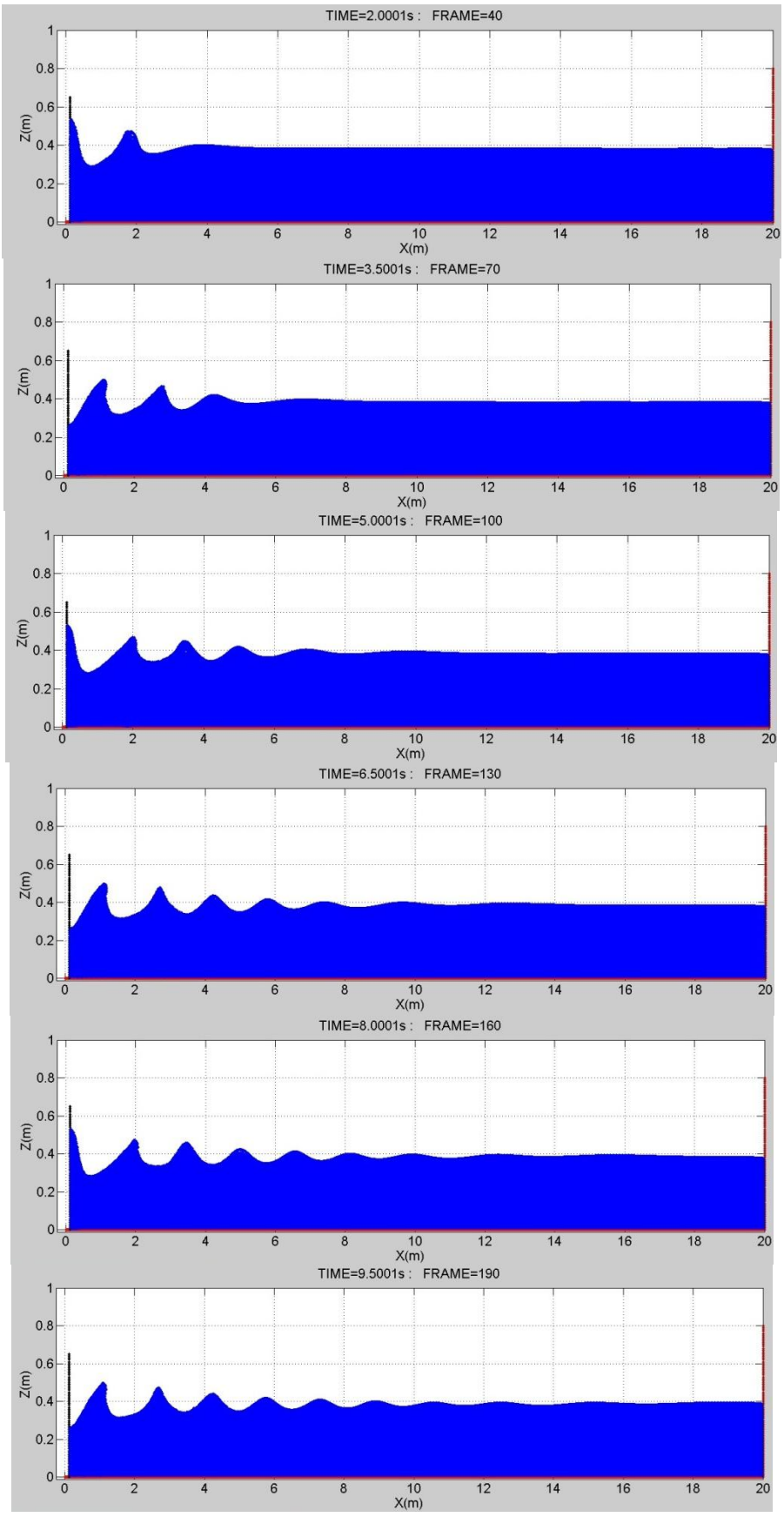

Figure 5.3. Simulation of the wave with T=1s and A=0.125m (case3)

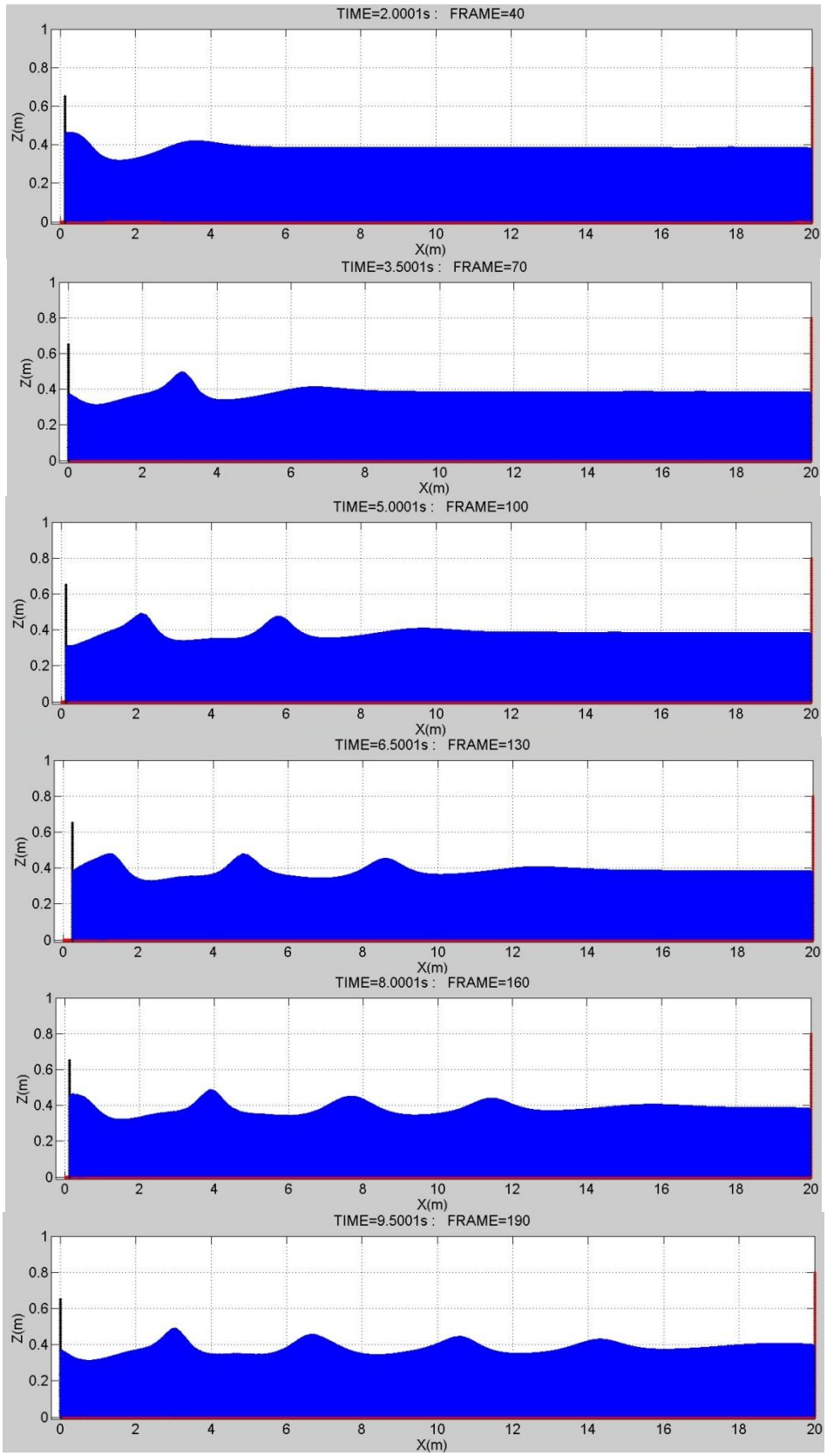

Figure 5.4. Simulation of the wave with T=2s and A=0.125m (case4)

5.3 Discussion of Results

The desired data such as water surface elevation and particle velocity are recorded at five locations to compare between the different four cases of simulated wave. The aim of this comparison is finding the largest wave and predict a desired position where will be optimum to generate power. The different points are represented in Fig.5.5.

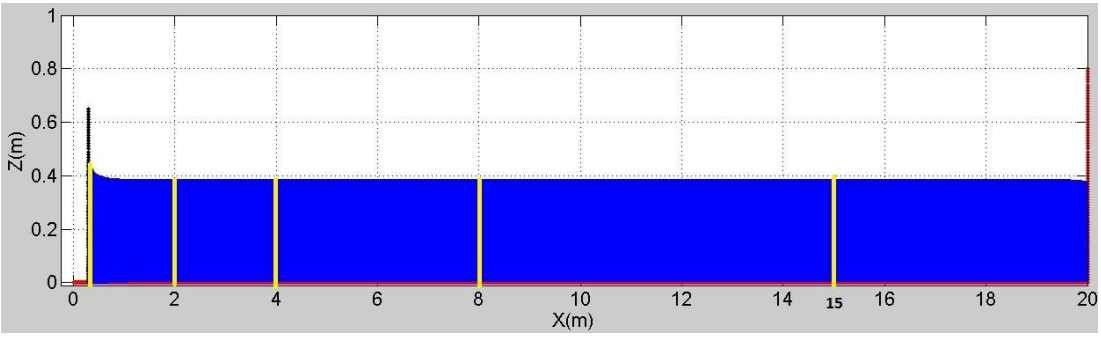

Figure 5.5. Four different locations for comparison between the four cases

5.3.1 Water Surface Elevation

The water surface elevation computed for the four various waves at five different locations during the wave propagation are shown in Figs.5.6-5.10 which are plotted by Matlab. Fig.5.6 compares wave height of the four different simulated cases for the closest particle to the wave maker. As the plot shows, the case 1 has maximum initial wave height in comparison with other cases due to lower period of wave maker and consequently a higher wave maker frequency. According to Fig.4.5, increasing the frequency results in an increasing the ratio of height wave to stroke of wave paddle. However, this enhancement is applicable as the frequency is less than 2 Hz. In addition Fig.5.6 indicates that an irregular flow is created on the free surface by the wave which has the initial highest height wave after wave breaking. Fig.5.7 depicts the wave of case 2 has maximum the wave height in comparison with other cases at

x=2. Also it can be seen that, although the case 4 was generated with minimum height wave initially, but it has the second rank in height wave now. This can be due to the fact that, there was no irregularity and breaking wave before the new waves is generated. In Fig.5.8, although the case 2 does not meet the maximum level at x=4m, but it has been the first rank in the wave height because of the amplitude of its wave maker is higher than case 4 in the same period. As shown in Figs.5.9-5.10, the wave of case 2 propagates with the highest height of wave at x=8m and x=15m.The wave of case 1 is larger than the wave of case 3 due to the case 1 created with the higher amplitude than the case 3 in the same period. As a result, the largest waves are case 2 the highest period (T=2s) and amplitude (A=0. 25m) of wave maker, case 4, case 1 and case 3 which generated with the lowest period (T=1s) and amplitude (A=0.125m) of wave maker respectively.

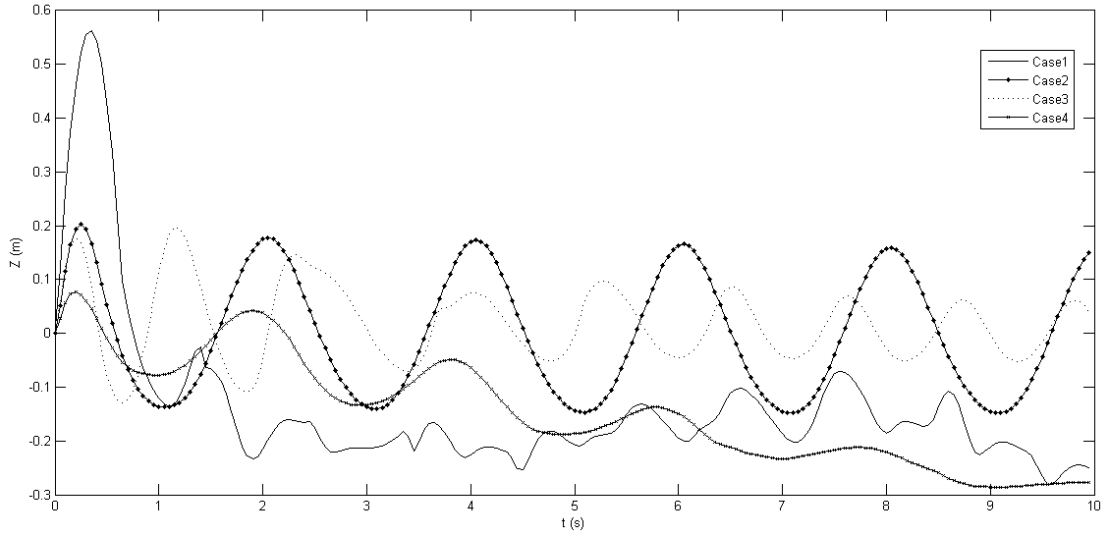

Figure 5.6. Comparison between water surface elevations of four waves at the closest particle to the wave maker

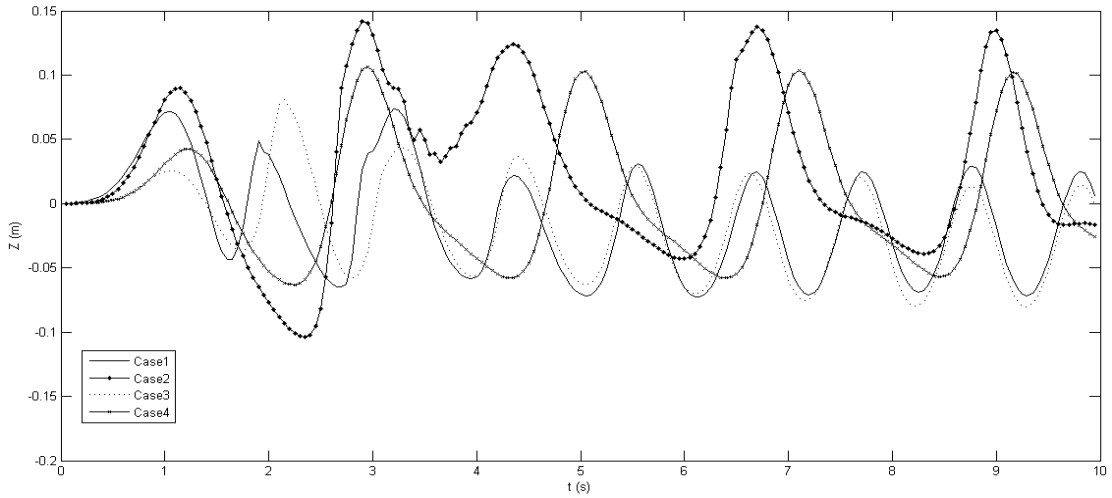

Figure 5.7. Comparison between water surface elevations of four waves at x=2

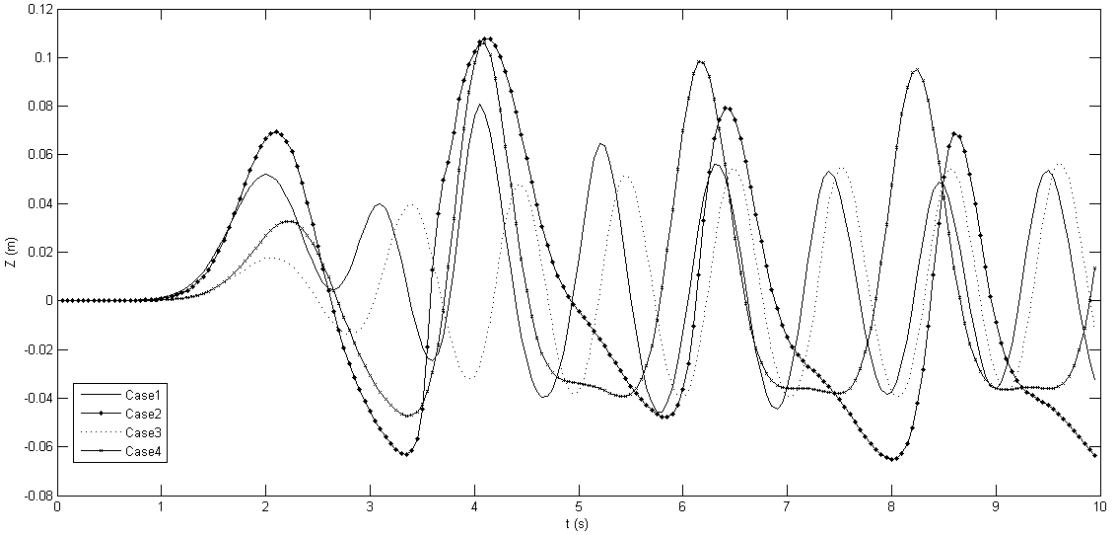

Figure 5.8. Comparison between water surface elevations of four waves at x=4

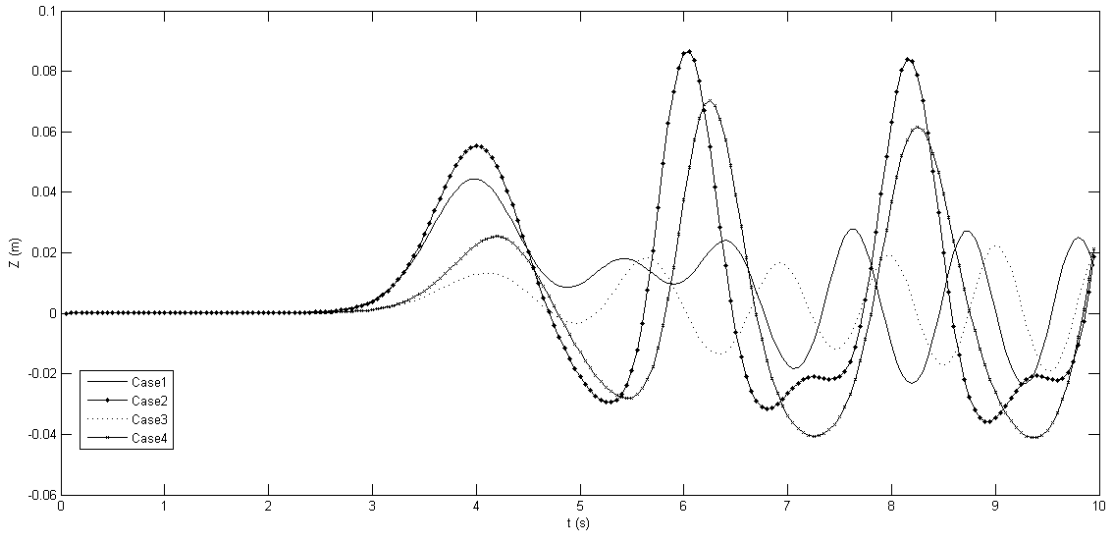

Figure 5.9. Comparison between water surface elevations of four waves at x=8

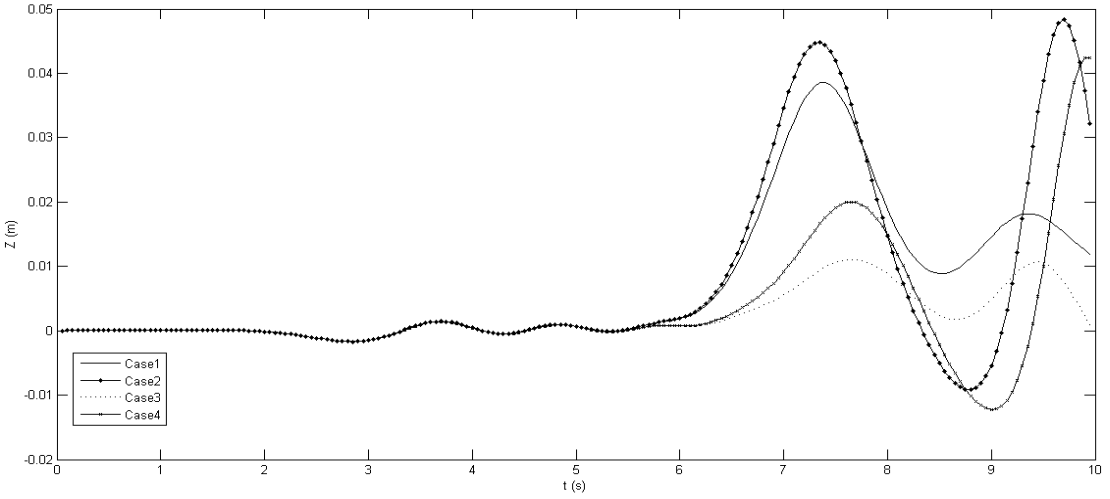

Figure 5.10. Comparison between water surface elevations of four cases of waves at x=15

5.3.2 Horizontal Particle Velocity

The Particle velocity in x direction of four various waves at different location can be plotted to compare kinematics. Fig.5.11, shows the horizontal velocity of the particle where located at the nearest to the wave maker on the free surface. In this case, two waves which created with less period (T=1s), have higher magnitude of velocity and also their behavior are highly irregular. Figs 5.12-5.15, represent the comparison the horizontal particle velocity between four waves at x=2m, x=4m, x=8m and x=15m

respectively on the free water surface. Figs 5.12-5.15 indicate that the case 2 and 4 have the higher horizontal particle velocity due to the case 2 and 4 have higher wave height.

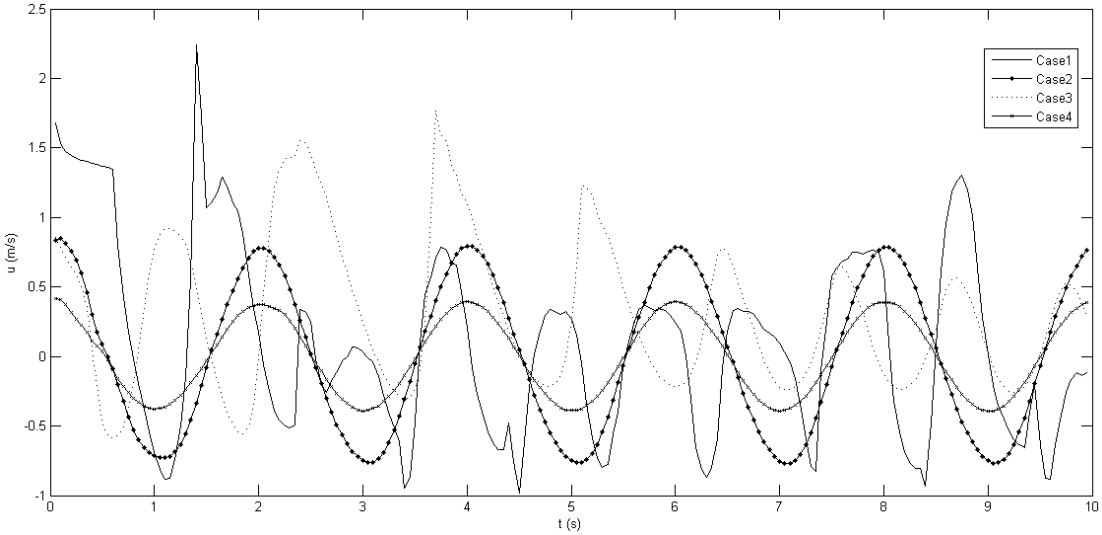

Figure 5.11. Comparison between horizontal particle velocity of four waves at (x,z)= (the closest particle to the wave maker, free surface)

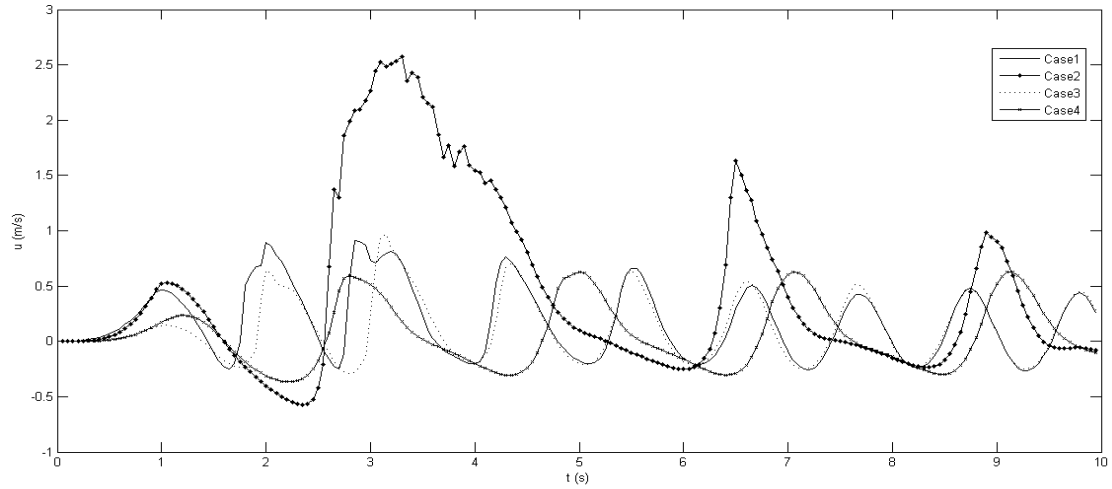

Figure 5.12. Comparison between horizontal particle velocity of four waves at (x,z)= (2m,free surface)

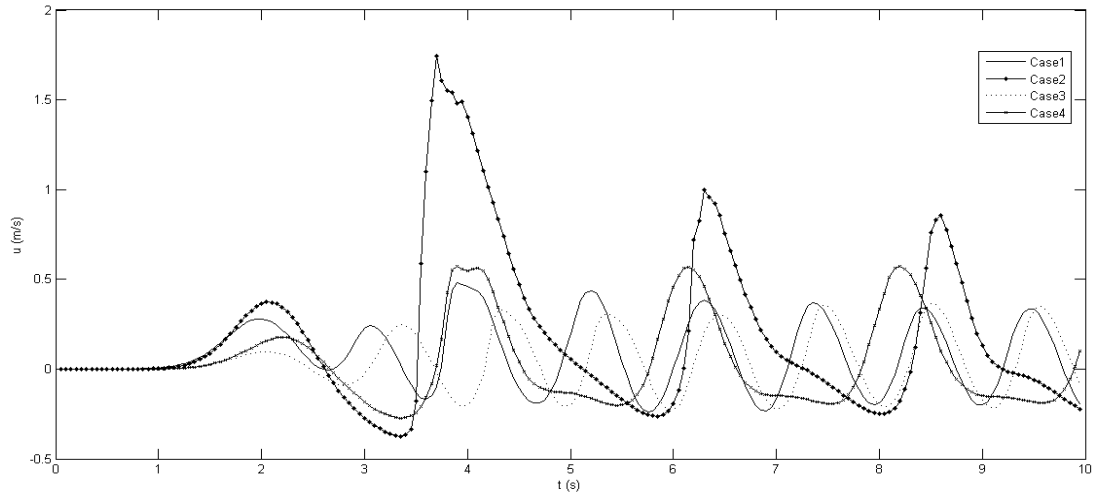

Figure 5.13. Comparison between horizontal particle velocity of four waves at (x,z)= (4m,free surface)

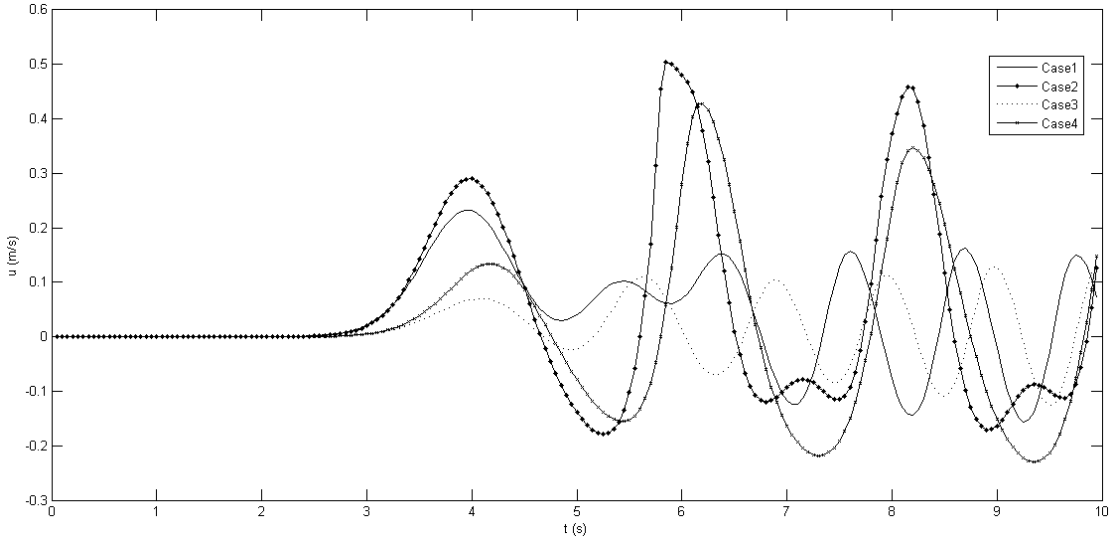

Figure 5.14. Comparison between horizontal particle velocity of four waves at (x,z)= (8m,free surface)

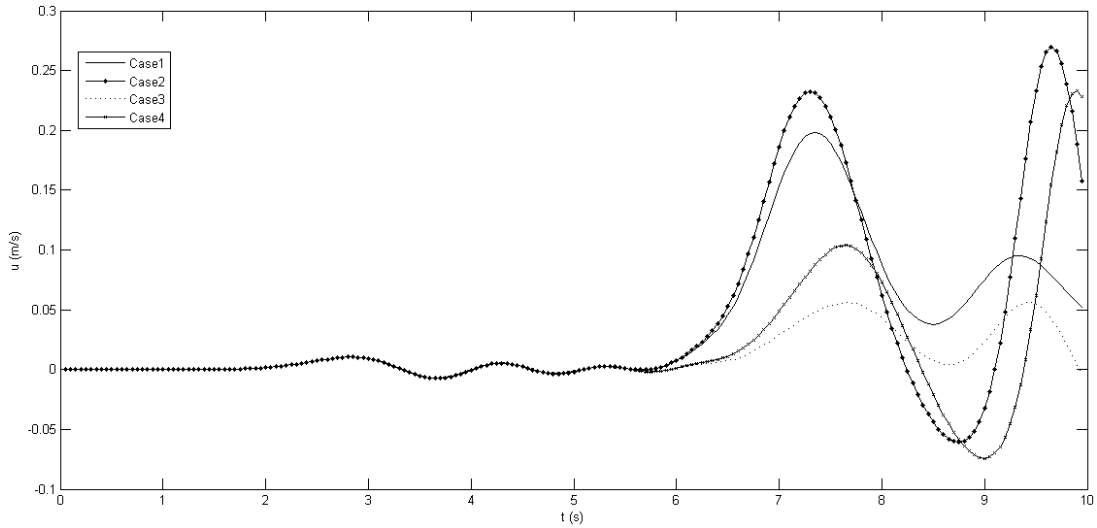

Figure 5.15. Comparison between horizontal particle velocity of four waves at (x,z)= (15m,free surface)

Moreover, the horizontal wave velocity in the two sub layers of the still water level where located 0.19 meter below the free surface and 0.09 meter above the bottom, are shown by Fig 5.16-5.25. As the Figs. 5.16 and 5.17 indicate the case 1 has the highest magnitude of velocity due to the behavior of this wave is chaotic in both of sub layers. Fig 5.18 and 5.19 shows this irregularity has been existed by case 1 at x=2. Also the velocity of case 1 increases after seventh second as z=0.19m below the free surface and after sixth second as z=0.09 m above the bottom. Figs 5.20-5.25 represent the comparison the horizontal particle velocity between four waves at x=4m, x=8m and x=15m respectively in both sub layers. According to Figs 5.20-5.25, the horizontal particle velocity of case 2 and case 4 which generated by higher period of wave maker are greater than the horizontal particle velocity of case 1 and 3; however the magnitude of their velocity are less than 0.4 m/s.

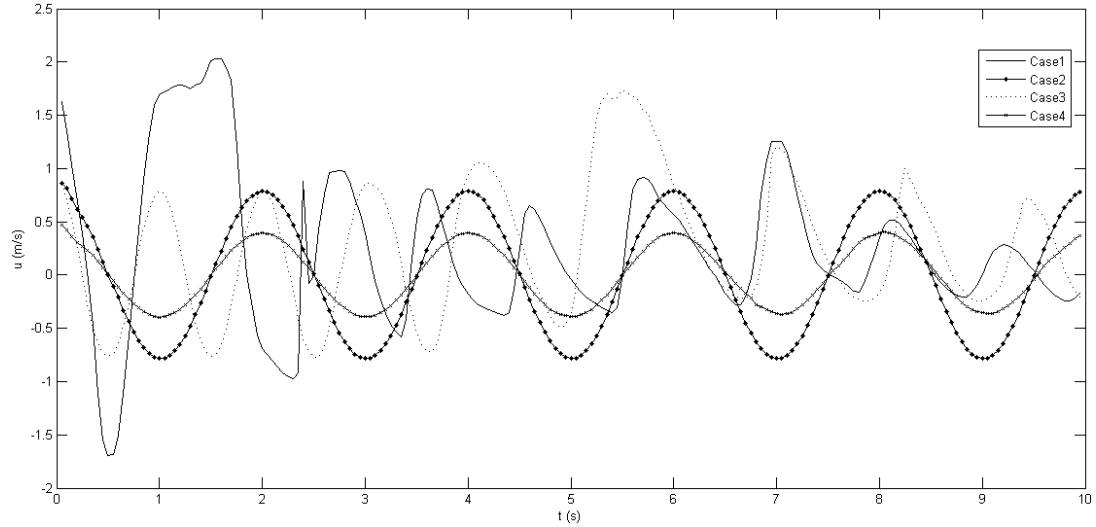

Figure 5.16. Comparison between horizontal particle velocity of four waves at (x,z)= (the closest particle to the wave maker, 0.19 meter below the free surface)

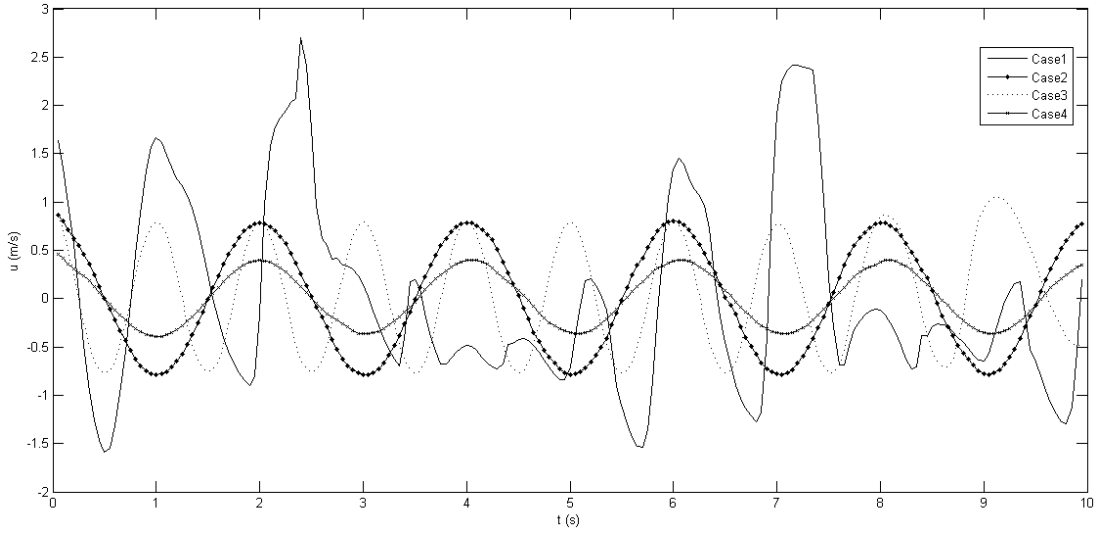

Figure 5.17. Comparison between horizontal particle velocity of four waves at (x,z)= (the closest particle to the wave maker, 0.09 meter above the bottom)

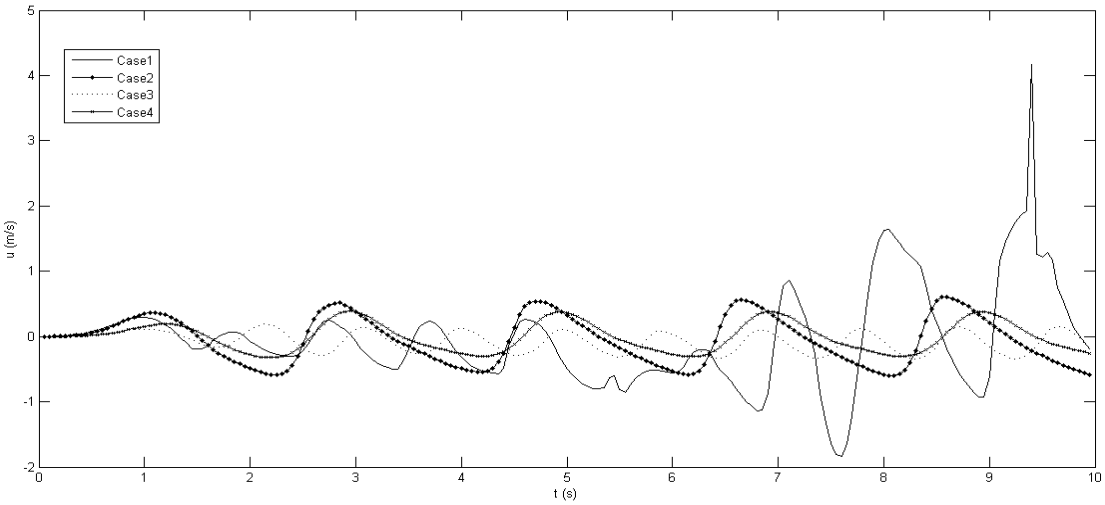

Figure 5.18. Comparison between horizontal particle velocity of four waves at (x,z)= (2m, 0.19 meter below the free surface)

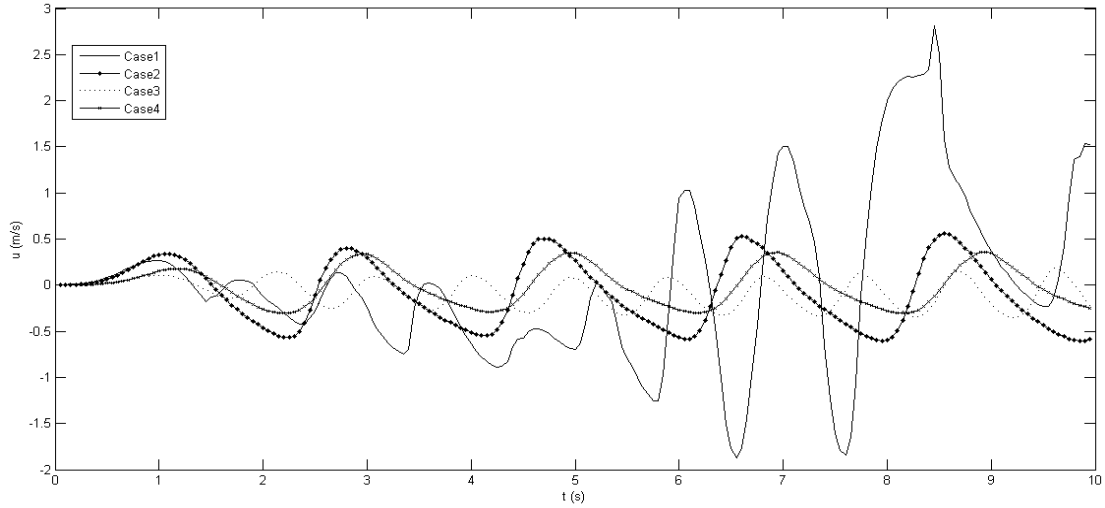

Figure 5.19. Comparison between horizontal particle velocity of four waves at (x,z)= (2m, 0.09 meter above the bottom)

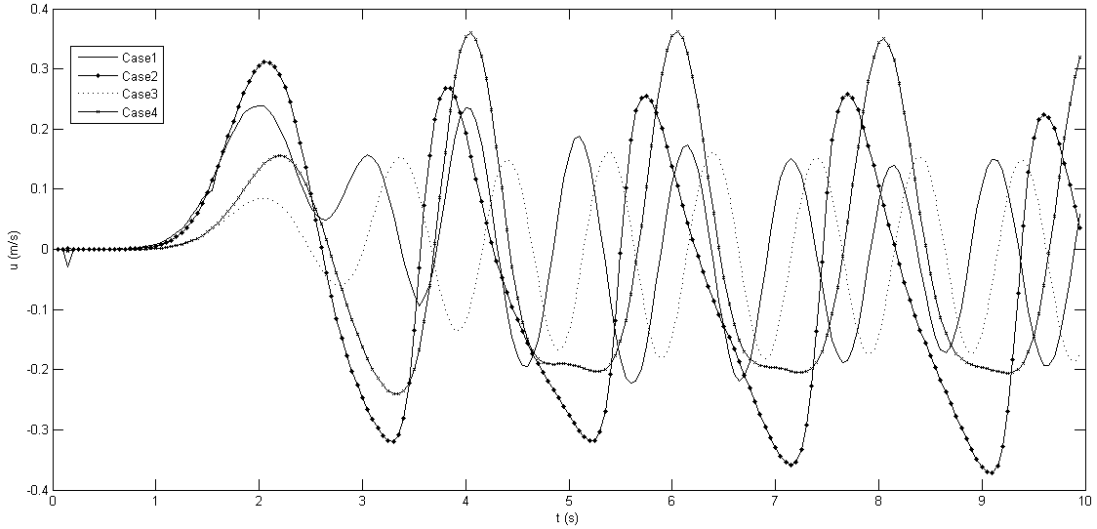

Figure 5.20. Comparison between horizontal particle velocity of four waves at (x,z)= (4m, 0.19 meter below the free surface)

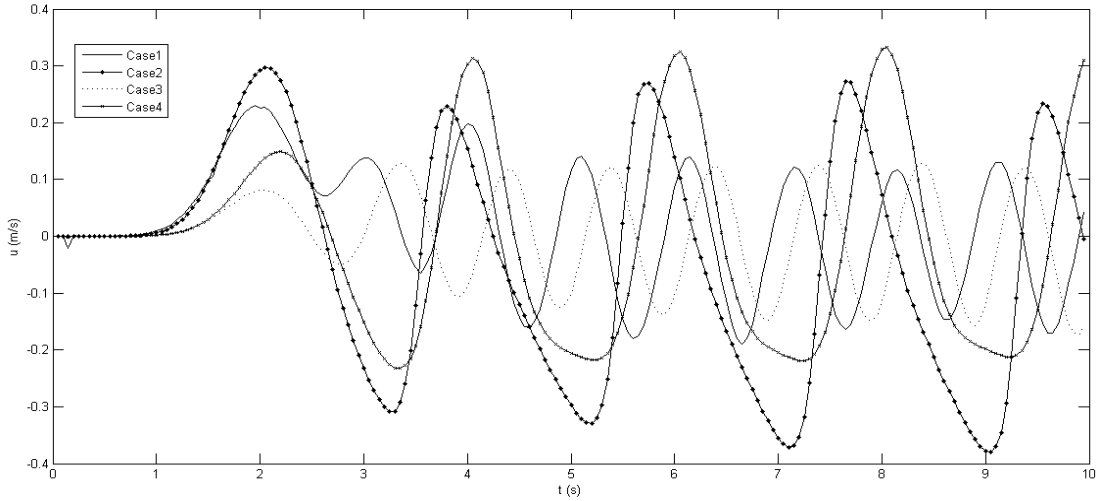

Figure 5.21. Comparison between horizontal particle velocity of four waves at (x,z)= (4m, 0.09 meter above the bottom)

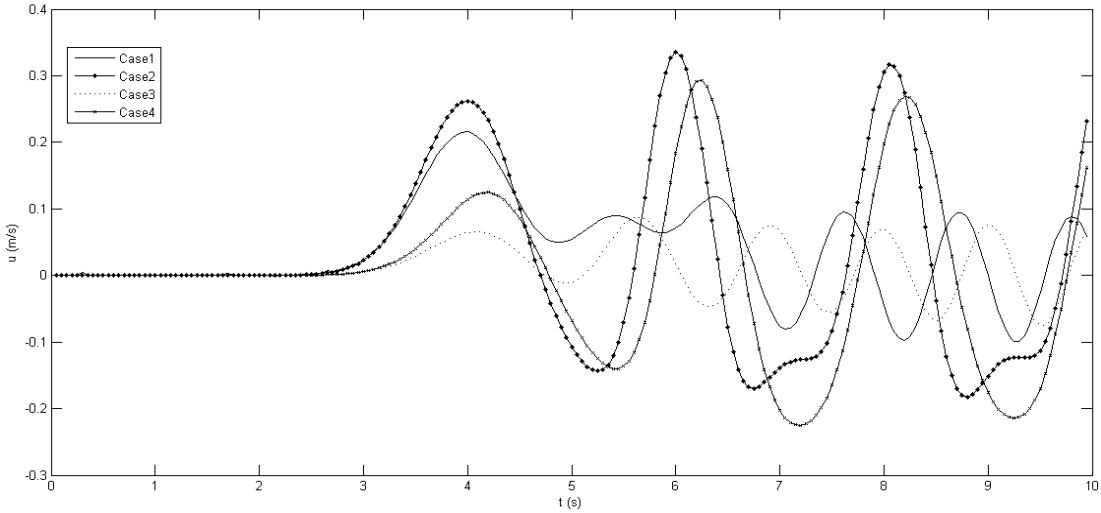

Figure 5.22. Comparison between horizontal particle velocity of four waves at (x,z)= (8m, 0.19 meter below the free surface)

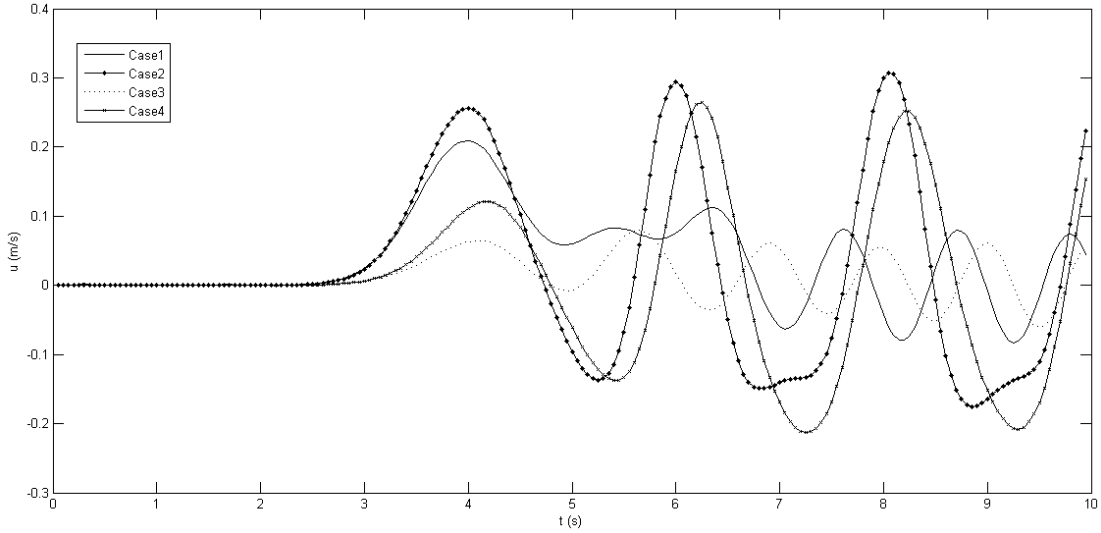

Figure 5.23. Comparison between horizontal particle velocity of four waves at (x,z)= (8m, 0.09 meter above the bottom)

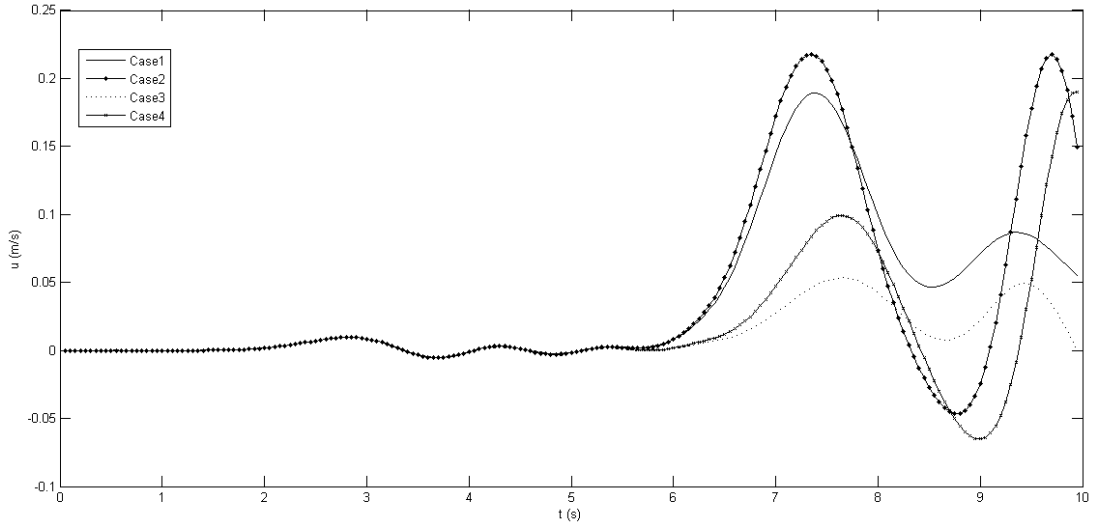

Figure 5.24. Comparison between horizontal particle velocity of four waves at (x,z)= (15m, 0.19 meter below the free surface)

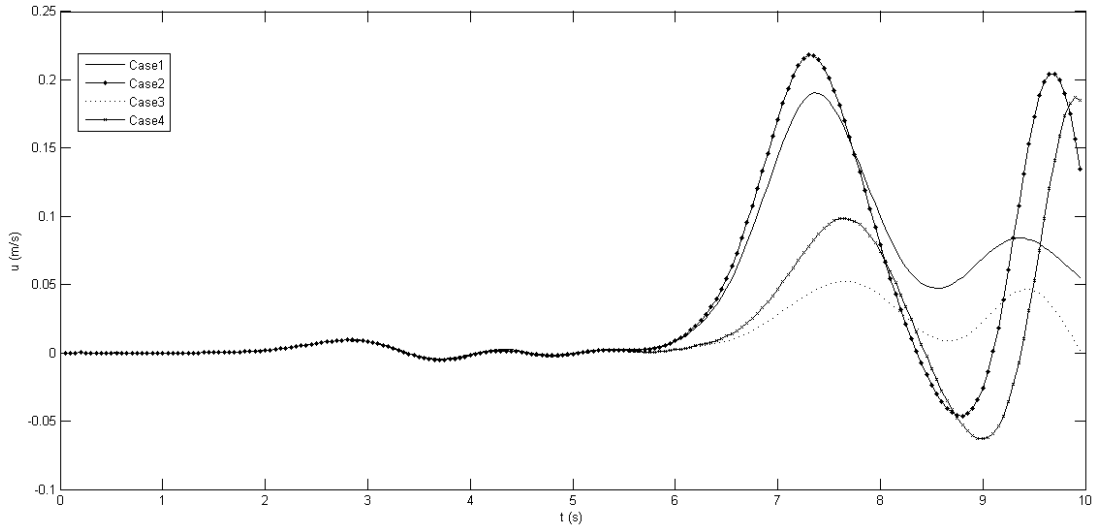

Figure 5.25. Comparison between horizontal particle velocity of four waves at (x,z)= (15m, 0.09 meter above the bottom)

5.3.3 Vertical Particle Velocity

The Particle velocity in z direction of four various waves at different location are shown in Figs 5.26-5.30. Fig.5.26 illustrates that the vertical particle velocity of case 1 is erratic at the nearest to the wave maker on the free surface and it hit a peak before first second. Fig 5.27 shows that case 2 has the highest magnitude of velocity and also its behavior are highly irregular at x=2m. Figs 5.28-5.30 indicate that the

vertical particle velocity of cases 2 and 4 are greater due to the case 2 and 4 generated with higher period and also they have the greater wave height at x=4m, x=8m and x=15m.

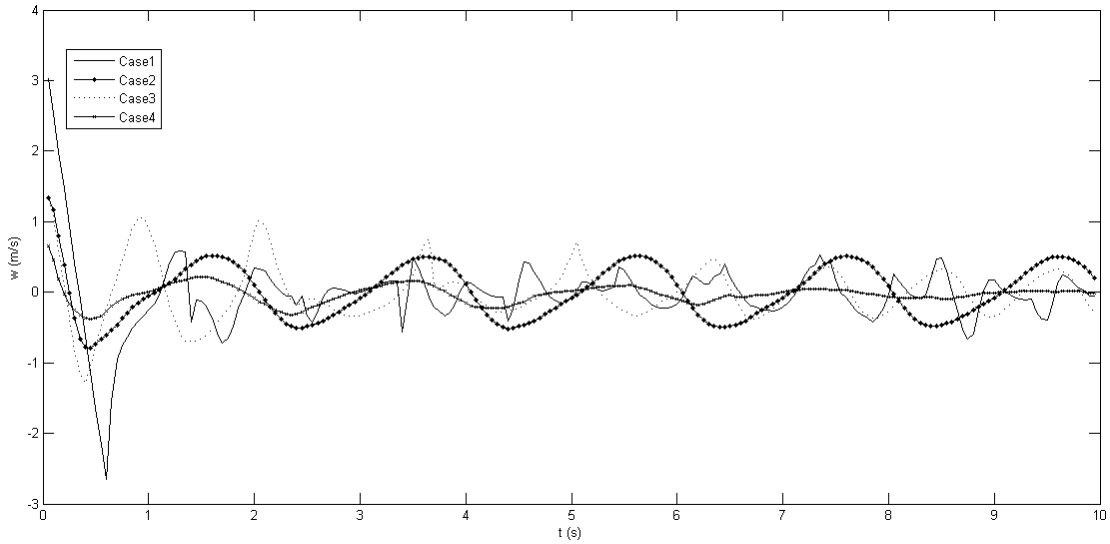

Figure 5.26. Comparison between vertical particle velocity of four waves at (x,z)= (the closest particle to the wave maker, free surface)

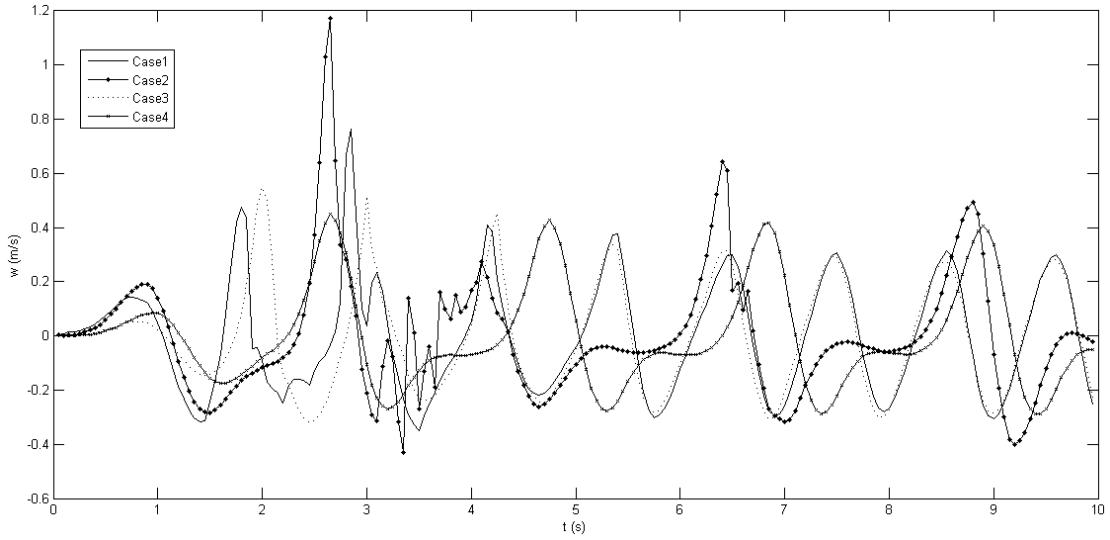

Figure 5.27. Comparison between vertical particle velocity of four waves at (x,z)= (2m, free surface)

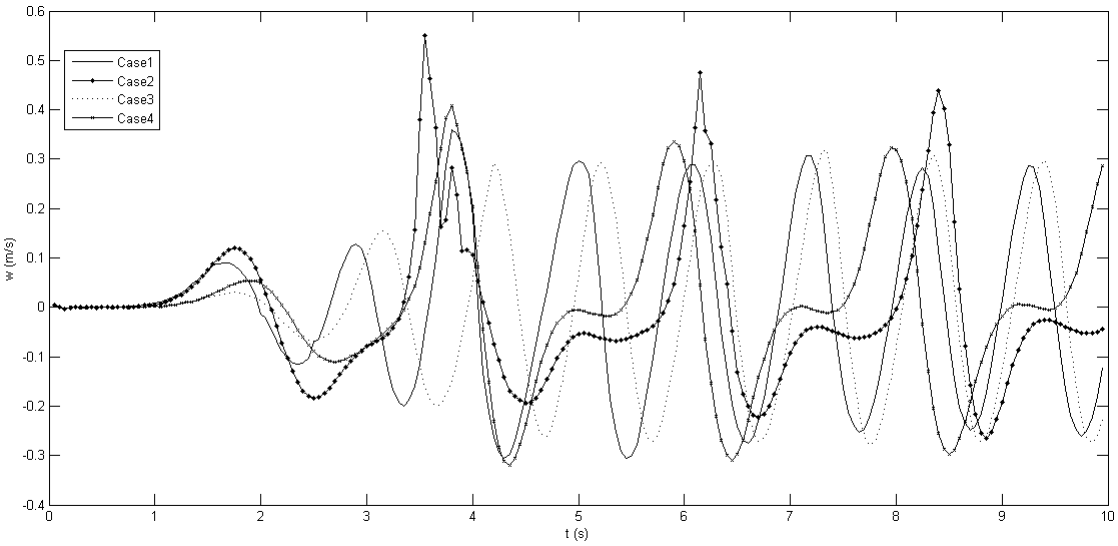

Figure 5.28. Comparison between vertical particle velocity of four waves at (x,z)= (4m, free surface)

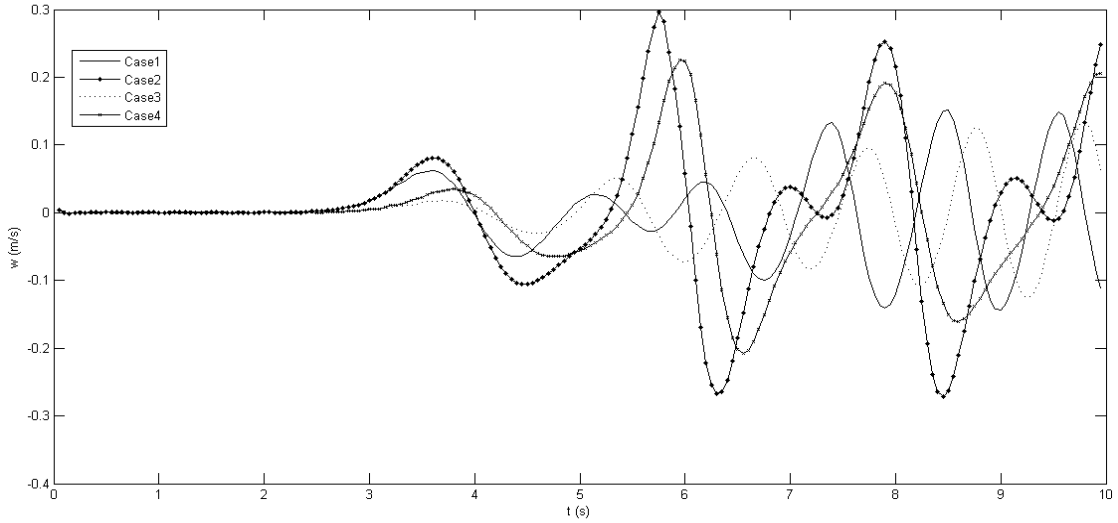

Figure 5.29. Comparison between vertical particle velocity of four waves at (x,z)= (8m, free surface)

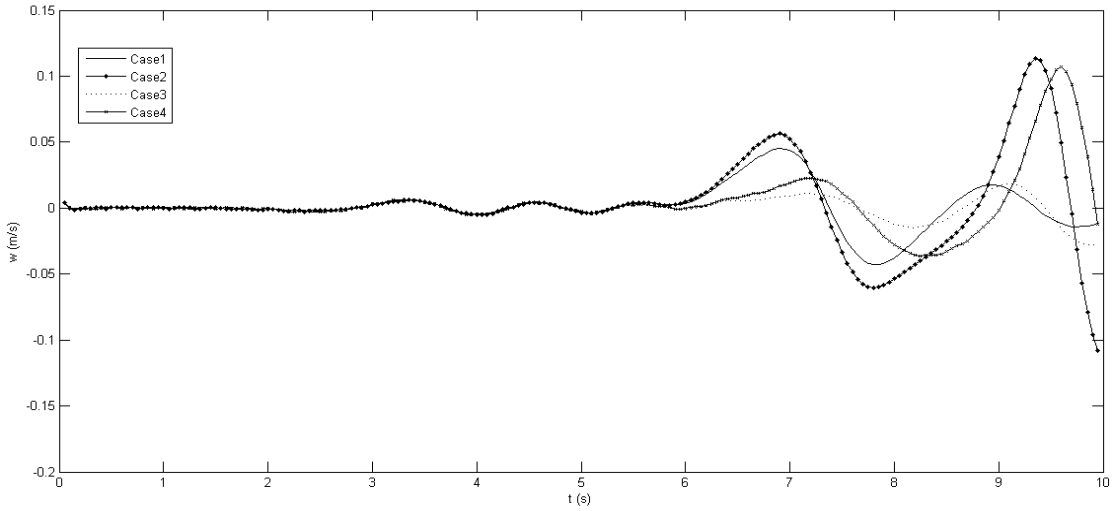

Figure 5.30. Comparison between horizontal particle velocity of four waves at (x,z)= (15m, free surface)

Similar to the horizontal particle velocity, the velocity of particle in z direction are plotted by Fig5.31-5.40 to compare vertical velocity of particle where located in sub layers where are 0.19 meter below the free surface and 0.09 meter above the bottom at x= 2m, x=4m, x=8m and x=15m. Generally speaking, these graphs illustrate that the magnitude of vertical particle velocity is decreasing as the position of sub layer is close to bottom except case 1 which is irregular at the nearest to the wave maker on the free surface. In addition the waves which generated with less period of wave maker such as cases 1 and 3 have greater vertical particle velocity. Also the amplitude of wave maker plays an important role in this case. For example, although the vertical particle velocity of cases 1 and 3 is greater but these magnitudes plummet after 4 meter and 2 meter downstream of the wave maker respectively in the both of sub layers.

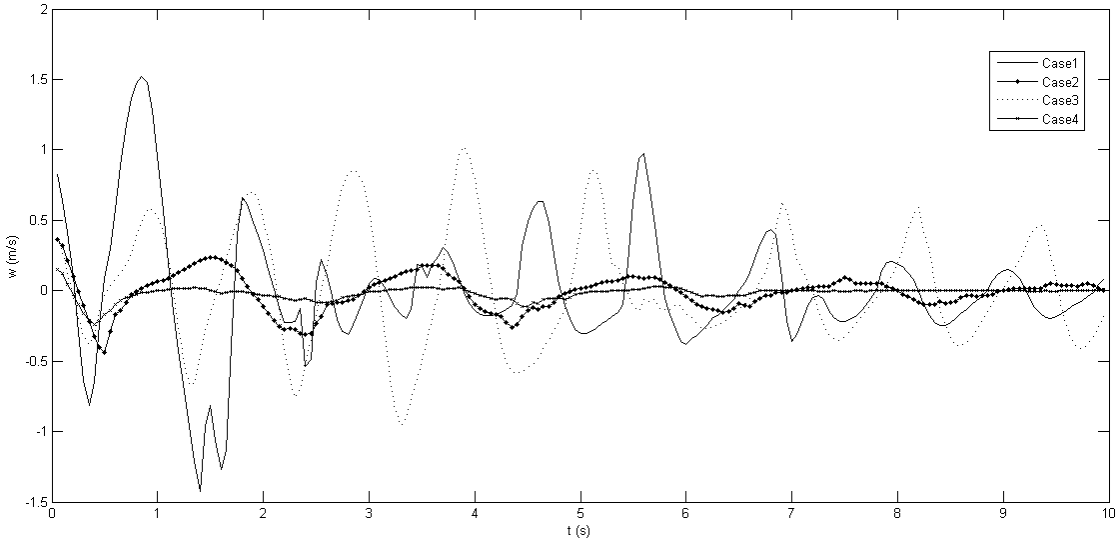

Figure 5.31. Comparison between vertical particle velocity of four waves at (x,z)= (the closest particle to the wave maker, 0.19 meter below the free surface)

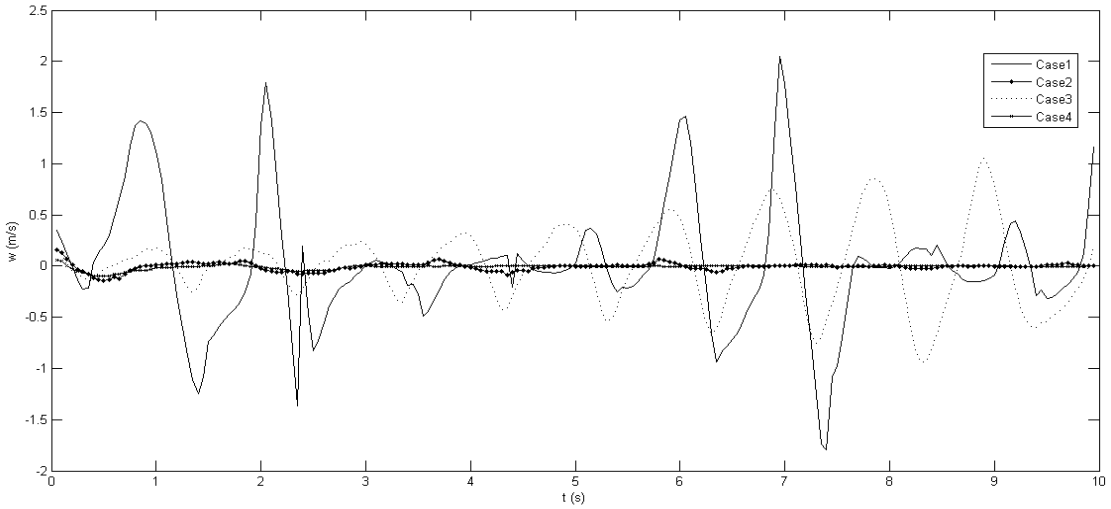

Figure 5.32. Comparison between vertical particle velocity of four waves at (x,z)= (the closest particle to the wave maker, 0.09 meter above the bottom)

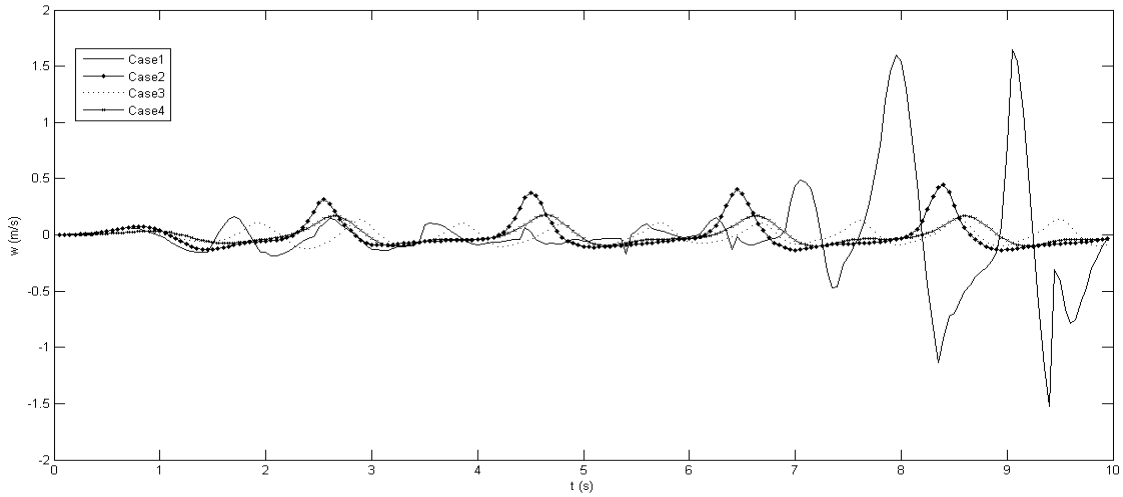

Figure 5.33. Comparison between vertical particle velocity of four waves at (x,z)= (2m, 0.19 meter below the free surface)

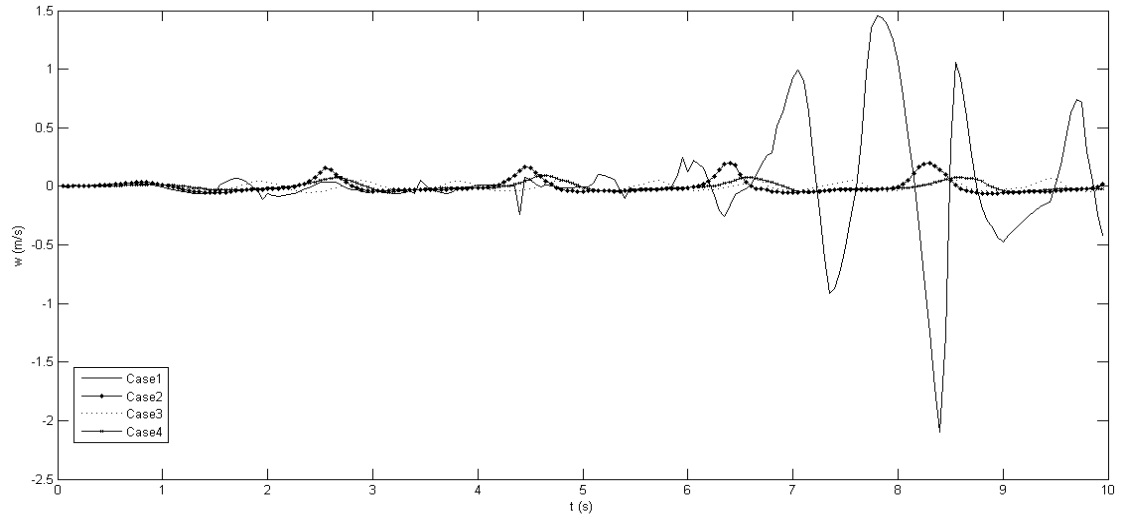

Figure 5.34. Comparison between vertical particle velocity of four waves at (x,z)= (2m, 0.09 meter above the bottom)

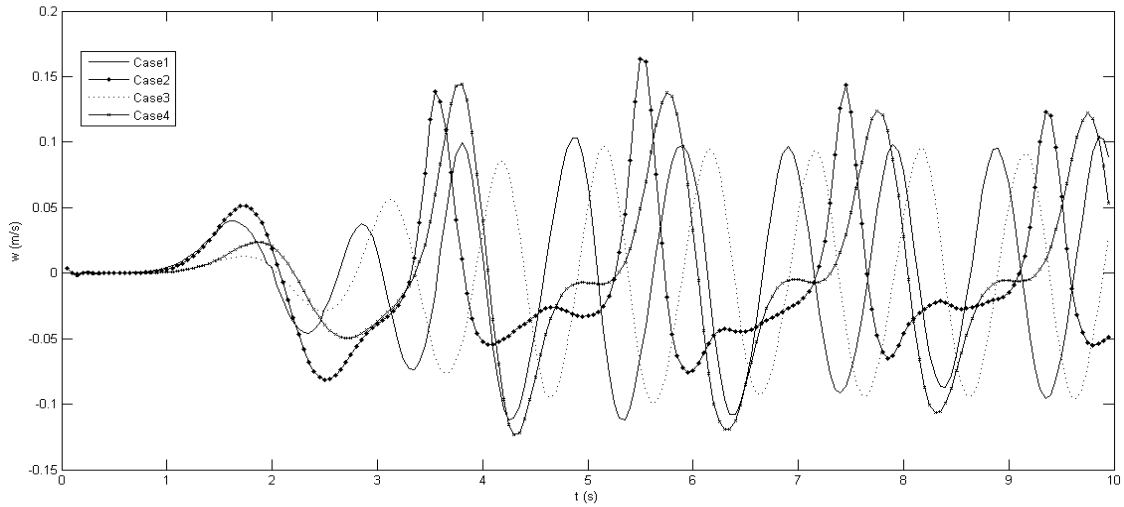

Figure 5.35. Comparison between vertical particle velocity of four waves at (x,z)= (4m, 0.19 meter below the free surface)

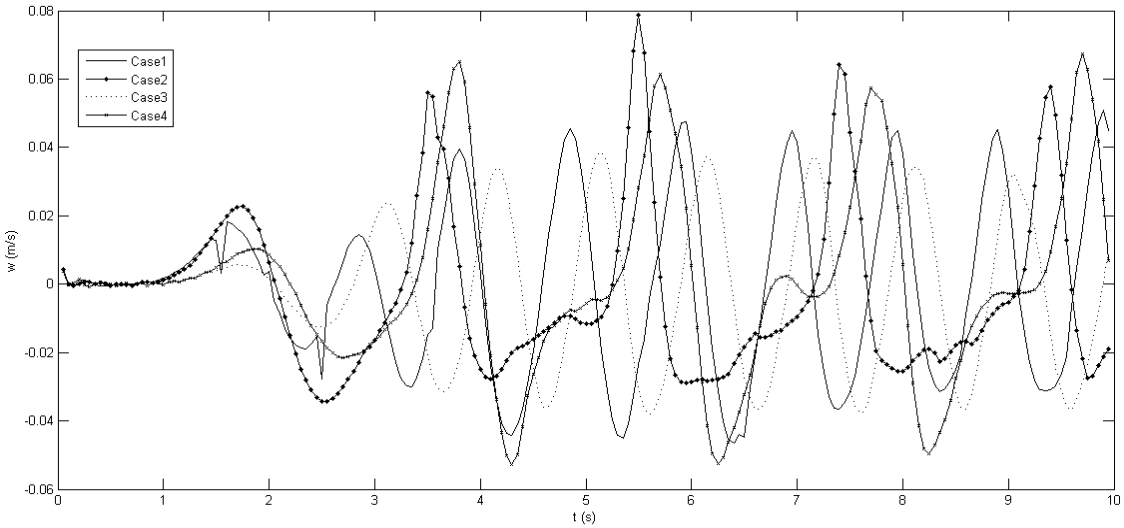

Figure 5.36. Comparison between vertical particle velocity of four waves at (x,z)= (4m, 0.09 meter above the bottom)

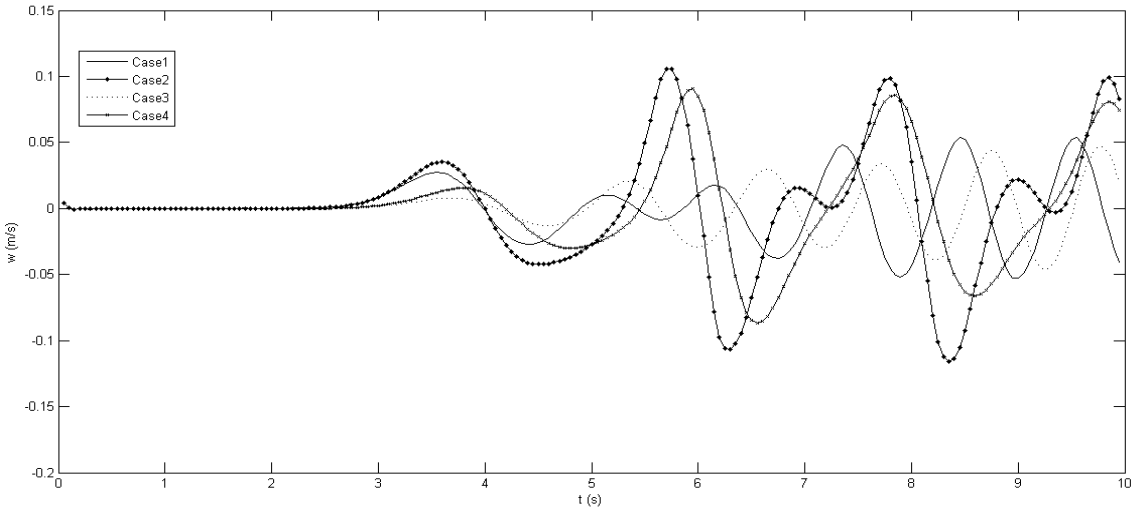

Figure 5.37. Comparison between vertical particle velocity of four waves at (x,z)= (8m, 0.19 meter below the free surface)

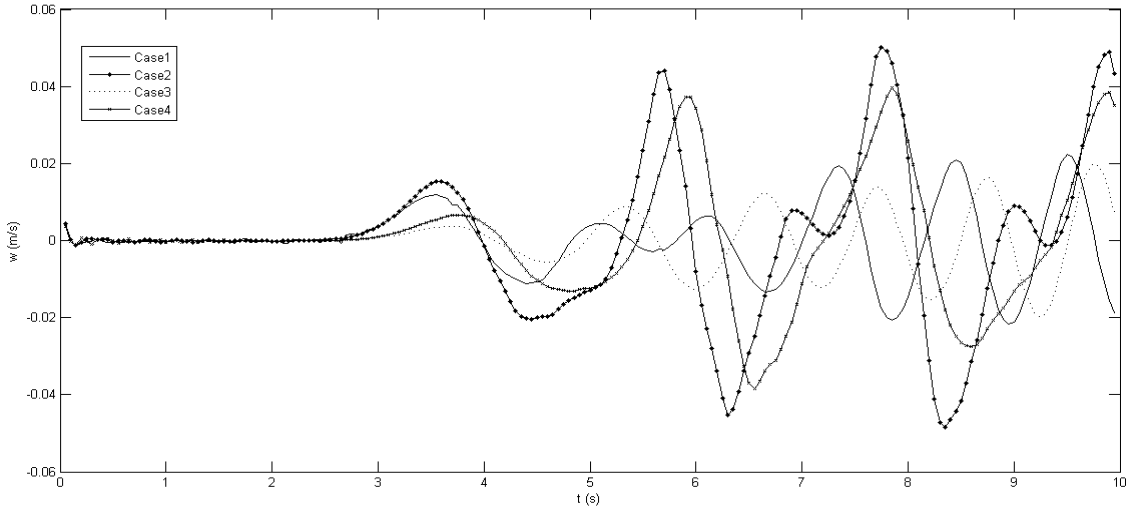

Figure 5.38. Comparison between vertical particle velocity of four waves at (x,z)= (8m, 0.09 meter above the bottom)

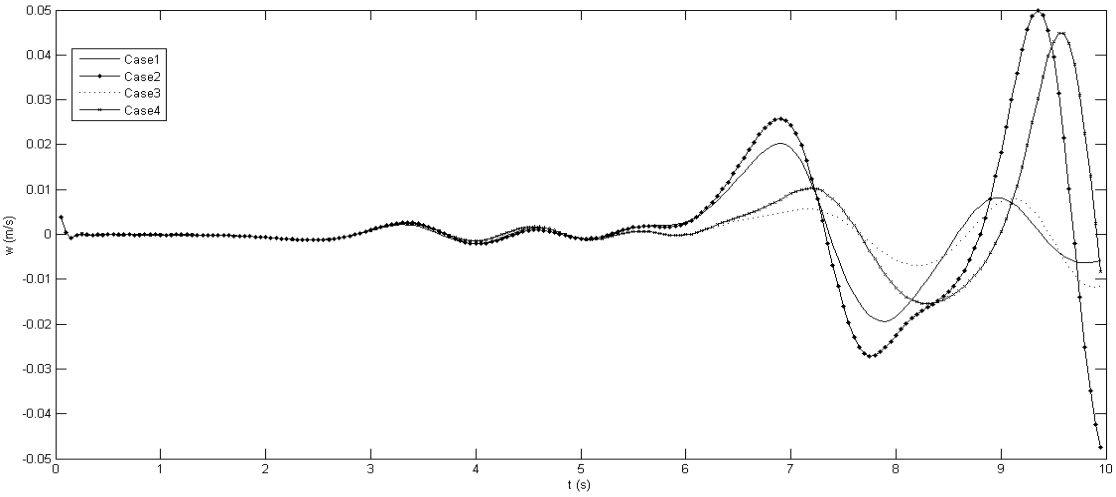

Figure 5.39. Comparison between vertical particle velocity of four waves at (x,z)= (15m, 0.19 meter below the free surface)

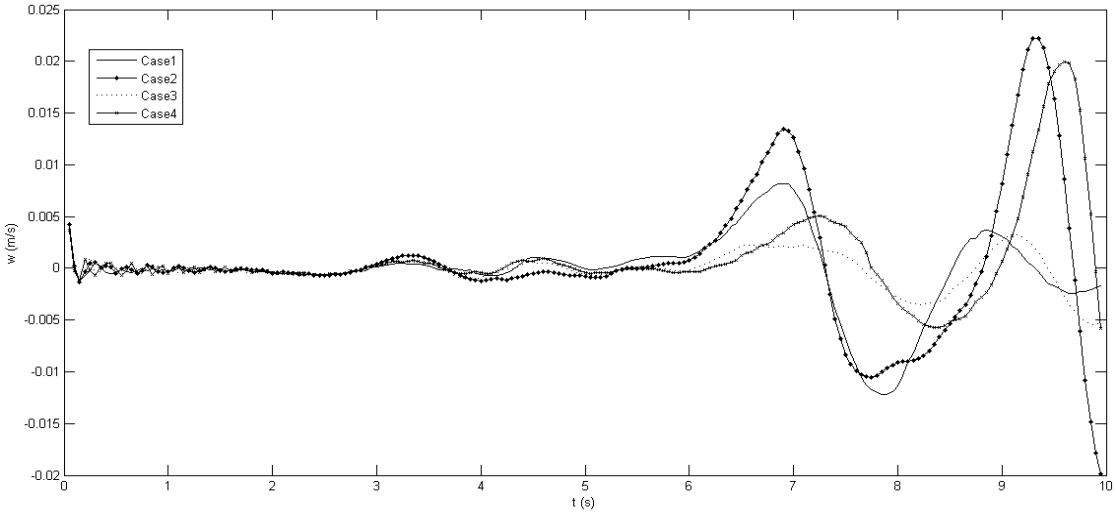

Figure 5.40. Comparison between vertical particle velocity of four waves at (x,z)= (15m, 0.09 meter above the bottom)

5.3.4 Total Energy

The summation of kinetic energy which produced by moving of water particles and potential energy which created by the free surface displacement will be total energy in a wave. Fig 5.41-5.42 represents kinetic energy and potential energy of fluid particles for all simulated cases. In both Figs 5.41-5.42, case 1 which generated with lower period (T=1s) and higher amplitude (A=0.25m) of wave maker has the most

kinetic and potential energy and consequently maximum total energy. Case 2 which created with higher period (T=2s) and higher amplitude (A=0.25m) of wave maker is located the second rank. However, kinetic and potential energy of Case 3 more than case4 until sixth second but kinetic and potential energy of case 4 is increasing more than case 3 after sixth second. Fig 5.43 shows Comparison between total energy of four waves. As result, total energy is increased by rising amplitude of wave maker and decreeing of wave maker period.

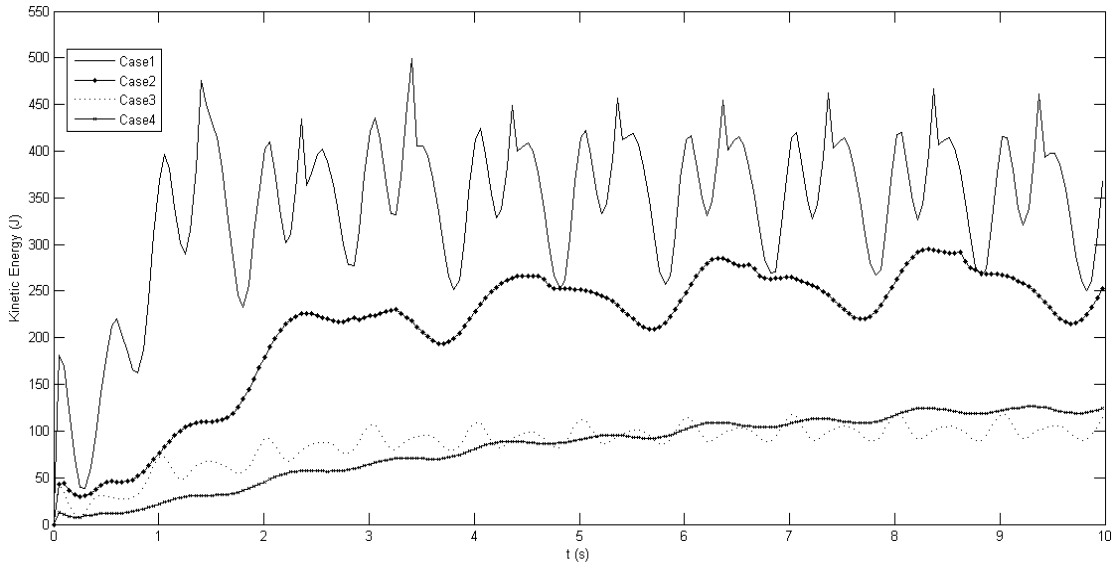

Figure 5.41. Comparison between kinetic energy of four waves

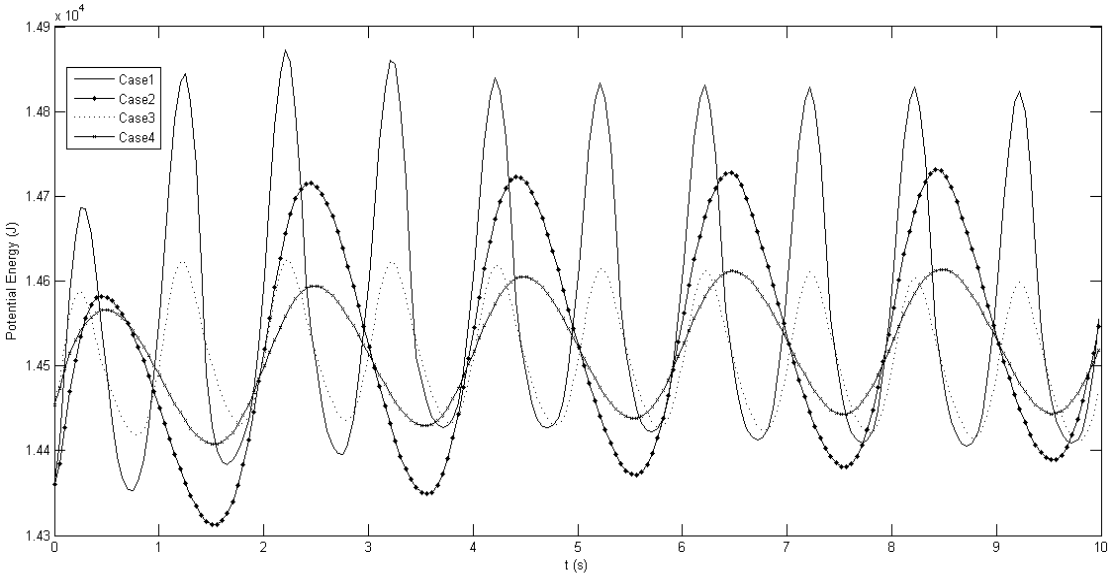

Figure 5.42. Comparison between potential energy of four waves

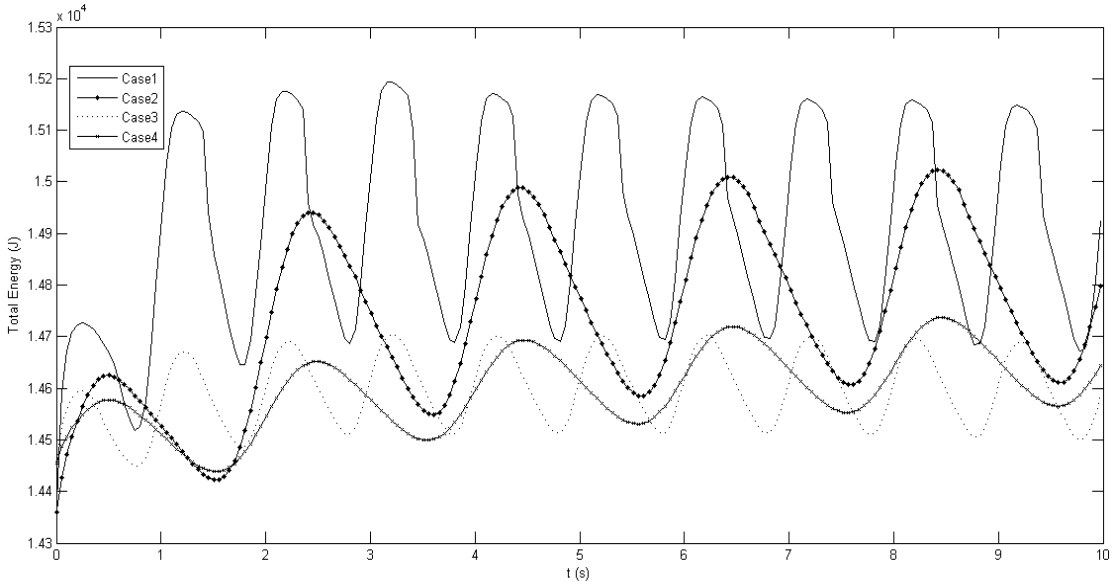

Figure 5.43. Comparison between total energy of four waves

Chapter 6

CONCLUSION AND FUTURE STUDY

6.1 Conclusion

This study has presented the numerical method to simulate the ocean wave as free surface phenomena. The focus on producing electricity from the ocean wave and marine current is a significant area of research. The numerical simulation provides a popular and proper way to understand flowing fluid behavior and floating devices. In this study, the smoothed particle hydrodynamics introduced as a mesh free method to model ocean waves. However, there are some disadvantages in numerical simulation with smoothed particle (SPH) method, thanks to the benefits of mesh less method, it can recommend to researchers for simulating free surface flow phenomena such as ocean wave and marine currents. The methodology named SPHysics which follows smoothed particle hydrodynamics formulation was studied and tested for modeling three types of the wave breaking. Then four various waves which generated by different period and amplitude of the piston type wave maker were modeled. Moreover, the water surface elevation at four points plotted. As a result, the height of wave depends on the frequency and stroke of wave maker. In addition, the horizontal and vertical velocities of particle where located 0.19 meter below the free surface and 0.09 meter above the bottom are analyzed. The results showed that the particle velocity was increasing by irregularity and rising height of wave and reduction in wave period. Also the magnitude of vertical particle velocity was decreasing as the position of sub layer was close to bottom. Finally, kinetic energy

which produced by moving of water particles and potential energy which created by the free surface displacement and total energy which is summation of kinetic and potential energy were examined. It was found when the amplitude of wave maker increases and the wave period decreases, total energy will increase.

6.2 Future Study

In this work, all the simulated cases were two dimensional and It is recommended to they can be executed by a 3D modeling and the new version of SPHysics called DualSPHysics. Moreover, it is good to compare simulation results with experimental results for observation of water behavior. In addition, it was assumed that the state equation of fluid is the weakly compressible. According to the SPHysics, an incompressible SPH code can be programmed and the new code applies in free surface phenomena problems.

REFERENCES

[1] International Energy Agancy (IEA), (2013). Energy Technology Initiatives 2013, 60

[2] Orogon State University, (2010). A primer on wave energy devices,

[3] Khaligh, A. & Omer, C. (2010). Energy Harvesting (Solar, Wind, and Ocean Energy Convesion Systems), 167-172, 227

[4] The European Marine Energy Center (EMEC) Website, http://www.emec.org.uk/marine-energy/wave-devices/

[5] Jones, W. J. & Ruane, M. (1977). Alternative Electrical Energy Sources, 11

[6] Charlier, R. H. (2003). A "Sleeper" Awakes: Tidal Current Power. Renewable and Sustainable Energy Reviews, p. 515-529

[7] Eurpean Commision. Non-nuclear Energy-JOULE ||, (1996). The Exploitition of Tidal and Marine Currents, 2

[8] https://wiki.manchester.ac.uk/sphysics/index.php/SPHYSICS_Home_Page

[9] Liu, G. R. & Liu, M. B. (2003). Smoothed Particle Hydrodynamics a mesh-free

particle method, World Scientific

[10] Liu, G. R. & Gu, Y. T. (2005). An Introduction to Mesh-free Methods and Their Programming. Chapter 2, 39-41,47,52

[11] Liu, M. B. & Liu, G. R. (2010). Smoothed Particle Hydrodynamics (SPH); an Overview and Recent Developments

[12] Lucy, L. B. (1977). A numerical approach to the testing of fusion process, Astronomical Journal, Vol. 88, pp. 1013-1024

[13] Gingold, R. A. & Monaghan, J. J. (1977). Smoothed Particle Hydrodynamics, Monthly Notice of the Royal Astronomical Society, Vol. 235, pp. 911-934

[14] Nayroles, B., Touzot, G. & Villon, P. (1992). Generalizing the finite element method: diffuse approximation and diffuse elements. Computational Mechanics, 10, 307-318

[15] Belytschko, T., Lu, Y.Y. & Gu, L. (1994). Element-free Galerkin methods. International Journal Numerical Methods Engineering. 37, 229-256

[16] Liu, W.K., Jun, S. & Zhang, Y. F. (1995). Reproducing kernel particle methods. International Journal Numerical Methods Engineering, 20, 1081-1106

[17] Atluri, S. N. & Zhu, T. (1998). A new meshless local Petrov-Galerkin (MLPG)

approach in computational mechanics. Computational Mechanics, 22, 117-127

[18] Liu, G. R. & Gu, Y. T. (1999) A point interpolation method. Proceedings of 4th Asia- Pacific Conference on Computational Mechanics, Dec. 1999, Singapore,1009-1014

[19] Liu, G. R. Gu, Y. T. & Wu, Y. L. (2003). A Mesh-free Weak-Strong form (MWS) method for fluid mechanics. Proceeding of International Workshop on Mesh-Free Methods

[20] Gingold, R. A. & Monaghan, J. J. (1982). Kernel estimates as a basis for general particle method in hydrodynamics, J. Computer. Physics, 46,429-53

[21] Monaghan, J. J. (1994). Simulating free surface flows with SPH. J. Computer. Physics. 110, 399–406

[22] Monaghan, J. J. & Kos, A. (1999). Solitary waves on a Cretan beach, J. Waterways Port Coastal Ocean Eng. 1111, 145-54

[23] Monaghan, J. J. & Kos, A. (2000). Scott Russell's wave generator Phys. Fluids, A 12, 622-30

[24] Dalrymple, R. A. & Rogers, B. D. (2006). Numerical modeling of water waves with the SPH method, Journal of Coastal Engineering, Vol. 53, pp. 141-147

[25] Narayanaswamy, M. S., Crespo, A. J. C., Gómez-Gesteira, M. & Dalrymple., R. A. (2010). SPHysics-FUNWAVE hybrid hodel for coastal wave propagation. J. Hydr. Res. 48(Extra Issue), 85–93

[26] De Leffe, M., Le Touzé, D. & Alessandrini, B. (2010). SPH modeling of shallow-water coastal flows. J. Hydr. Res. 48(Extra Issue), 118–125

[27] Rogers, B. & Dalrymple, R. A. (2004). SPH modeling of breaking waves, 29th International Conference on Coastal Engineering, pages 415-427

[28] De Serio, F. & Mossa, M. (2006). Experimental study on the hydrodynamics of regular breaking waves, J. of Coastal Engineering, vol. 53, pp. 99-113

[29] Khayyer, A., Gotoh, H. & Shao, S. D. (2008). Corrected incompressible SPH method for accurate water-surface tracking in breaking waves, Journal of Coastal Engineering, Vol 55 (3), pp. 236-250

[30] Gomez-Gesteira, M., Rogers, B. D., Dalrymple, R. A. & Crespo, A. J. C. (2010). State-of-the-art of classical SPH for free-surface flows. J. Hydr. Res. 48, 6–27

[31] Capone, T., Panizzo, A. & Monaghan, J. J. (2010). SPH modeling of water waves generated by submarine landslides. J. Hydr. Res.48, 80–84

[32] Lee, E. S., Moulinec, C., Xu, R., Violeau, D., Laurence, D. & Stansby, P. (2008).Comparisons of weakly compressible and truly incompressible

algorithms for the SPH mesh free particle method. J. Comput. Phys. 227, 8417–8436

[33] Hughes, J. P., David, I. & Graham, D. I. (2010). Comparison of incompressible and weakly-compressible SPH models for free-surface water flows. J. Hydr. Res. 48, 105–117

[34] López, D., Marivela, R. & Garrote, L. (2010). SPH model applied to hydraulic structures: A hydraulic jump test case. J. Hydr. Res. 48, 142–158

[35] Groenenboom, P. H. L. & Cartwright, B. K. (2010). Hydrodynamics and fluid-structure interaction by coupled SPH-FE method. J. Hydr. Res. 48, 61–73

[36] Marongiu, J. C., Leboeuf, F., Caro, J. & Parkinson, E. (2010). Free surface flows simulations in pelton turbines using an hybrid SPH-ALE method. J. Hydr. Res. 48(Extra Issue), 40–49

[37] Hérault, A., Bilotta, G. & Dalrymple, R.A. (2010) SPH on GPU with CUDA. J. Hydr. Res. 48, 74–79

[38] Lee, E. S., Violeau, D., Issa, R. & Ploix, S. (2010). Application of weakly compressible and truly incompressible SPH to 3D water collapse in waterworks. J. Hydr. Res. 48, 50–60

[39] Maruzewski, P., Le Touzé, D., Oger, G. & Avellan, F. (2010). SPH high-

performance computing simulations of rigid solids impacting the free-surface of water. J. Hydr. Res. 48, 126–134

[40] DUALSPHysics : http://dual.sphysics.org/

[41] Vacondio, R., Mignosa, P. & Pagani, S. (2013) 3D SPH numerical simulation of the wave generated by the Vajont rockslide. Advances in Water Resources, 59, 146-156

[42] University of Heidelberg, Institute of Theoretical Astrophysics, http://www.ita.uni-heidelberg.de/~dullemond/lectures/num_fluid_2011

[43] Monaghan, J. J. (2005). Smoothed particle hydrodynamics, Rep. Progress Phys., 68, 1703-1759

[44] Monaghan, J. J. (1989). On the problem of penetration in particle methods. Journal of Computational Physics 82, 1–15

[45] Monaghan, J. J. (1992) Smoothed particle hydrodynamics. Annual Review of Astronomy and Astrophysics 30, 543–574

[46] Lo, E. Y. M. & Shao, S. (2002). Simulation of near-shore solitary wave mechanics by an incompressible SPH method. Applied Ocean Research 24, 275–286

[47] Gotoh, H., Shibihara, T. & Hayashii, M. (2001). Sub-particle-scale model for the MPS method-Lagrangian flow model for hydraulic engineering, Computational Fluid Dynamics Journal 9, 339–347

[48] Dilts, G.A. (1999). Moving-least-squares-particle hydrodynamics – I. Consistency and stability, International Journal for Numerical Methods in Engineering 44, 1115–1155

[49] Colagrossi, A. & Landrini, M. (2003). Numerical simulation of interfacial flows by smoothed particle hydrodynamics. Journal of Computational Physics 191, 448–475

[50] Bonet, J. & Lok, T. S. L. (1999). Variational and momentum preservation aspects of smoothed particle hydrodynamic formulations. Computer Methods in Applied Mechanical Engineering 180, 97–115

[51] Vila, J. P. (1999). On particle weighted methods and smooth particle hydrodynamics. Mathematical Models and Methods in Applied Sciences 9, 161–209

[52] Liu, W., Li, S. & Belytscho, T. (1997). Moving least square Kernel Galerkin method (I) methodology and convergence. Computer Methods in Applied Mechanics and Engineering 143, 113–154

[53] Verlet, L. (1967). Computer experiments on classical fluids. I. Thermodynamical properties of Lennard-Jones molecules. Physical Review 159,

98–103

[54] Beeman, D. (1976). Some multistep methods for use in molecular dynamics calculations. Journal of Computational Physics 20, 130–139

[55] Crespo, A. J. C., Gomez-Gesteira & Dalrymple, R. A. (2007). Boundary conditions generated by dynamic particles in SPH methods, Computers and Materials, Continua 5,173–184

[56] Hughes, J. & Graham, D. (2010). Comparison of incompressible and weakly-compressible SPH models for free-surface water flows. Journal of Hydraulic Research 48, 105–117

[57] Hansen, M. P. (2008). The virtual wave flume-with the SPH method, Ch 5, 69

[58] Ergin, A. (2009) Costal Engineering, ch 1&4

[59] Sorensen, R.,M. (1993). Basic Wave Mechanics for Coastal and Ocean Engineers. John Wiley and Sons

[60] Scott, L., Douglass, and Krolak, J. (2008). Highways in the Coastal Environment: Second Edition, 33-54

[61] http://www.tulane.edu/~bianchi/Courses/Oceanography

[62] Grilli, S.,T., Svendsen, I.,A. and Subramanya, R. (1997). Breaking criterion and characteristics for solitary waves on slopes, J. Waterway Port Coastal and Ocean Engineering, 123(3), 102-112

[63] Frigaard, P., Hogedor, M., Charistensen, M. (1993). Wave generation theory, 5-35